Gravity Recovery by LN-93 Strapdown Airborne Gravity System— A Comparison of Different Vector Gravimetry Approaches Based on Simulations

by

Jin Wang

Report No. 439

Geodetic Science and Surveying
Department of Civil and Environment Engineering and Geodetic Science
The Ohio State University
Columbus, Ohio 43210-1275

February 1997

Gravity Recovery by LN-93 Strapdown Airborne Gravity System— A Comparison of Different Vector Gravimetry Approaches Based on Simulations

by

Jin Wang

Report No. 439

Geodetic Science and Surveying
Department of Civil and Environment Engineering and Geodetic Science
The Ohio State University
Columbus, Ohio 43210-1275

February 1997

SUMMARY

Following a brief history of gravity determination, the general principle and the basic requirement for airborne implementation is presented. The difficulty of extracting gravity information from the time-synchronized series of inertial navigation system (INS) and global positioning system (GPS) measurements is due to the small signal-to-noise ratio. A spectral analysis is performed according to the error spectrum of the system using information from the specification of the Litton LN-93 strapdown system and the power spectral density (PSD) parameter model for GPS-derived acceleration error obtained from flight test data. It is shown that, at the constant aircraft speed of 360 km/hr, vector gravimetry can be performed successfully in the frequency range of 2.99×10^{-4} Hz to 2.23×10^{-3} Hz, i.e., the wavelength from 45 km to 334 km for a baseline gravity model. Similarly the spectral analyses for both smooth and rough gravity signature are also performed. The dominating error sources for airborne gravimetry at different frequency ranges are discussed.

The most common two approaches, Kalman filtering and wave estimation, are considered and compared here. In Kalman filtering, a stochastic model is used to describe the gravity disturbance, while in wave estimation, a deterministic model, usually a simple function, is anticipated to approximate the gravity disturbance for a short time interval. For the practical application of vector gravimetry, a full state, 27th-order system model is taken in the Kalman filter by modeling the gravity disturbance with a 3rd-order Gauss-Markov process. As to the wave estimation, a separate algorithm for the horizontal channels is designed considering the weak observability in short time and the feature of deterministic description for the gravity disturbance. The most appropriate estimation cycle for the wave estimation is found to be about 80 seconds. Based on the linear principle, it is proposed here to treat the calibration residual at the initial alignment to be of one single error while regarding the others as zero. In this way, one can avoid the difficulty of estimating and distinguishing each individual initial error.

Considering only the essential errors of LN93 inertial system and differential GPS phase measurements, and assuming the aircraft flies at a constant speed, the combined system is simulated thoroughly. The gravity disturbance is also simulated using a sum of two 3rd-order Gauss-Markov models. Finally with the simulated data, two methods, Kalman filtering and wave estimation, are applied to recover the gravity information. The performance with different trajectories and under different circumstances is discussed. The results show that an accuracy of 1--3 mgal (RMS) is achievable within one hour with a medium accuracy strapdown airborne gravity system. It is concluded that the Kalman filter is slightly superior to wave estimation when dealing with the rough gravity signature. This is partially because wave estimation cannot properly account for the contradiction of good deterministic description, which requires a short estimation cycle, and state convergence, which holds for a long period.

ACKNOWLEDGMENTS

This work was supported by Air Force Philips Laboratory Contract No. F19628-95-K-0020, Ohio State Research Foundation Project No. 731618. I wish to thank Dr. Christopher Jekeli for his continuous encouragement and intellectual discussions.

TABLE OF CONTENTS

Page

LIST OF FIGURES

LIST OF TABLES

1 INTRODUCTION

1.1 Background

The recovery of the Earth's Gravity information has been an important pursuit for a variety of geodetic and geophysical applications. Conventional methods with static gravimeters and astronomical determination of the deflection of the vertical have achieved a high accuracy for the determination of the gravity vector at discrete points, but are extremely time consuming and expensive. Some remote and mountainous areas can not be well covered and there still remain gaps to be filled. Due to the prohibitive costs of satellite gravity mapping missions, it is encouraged to consider moving-base vector gravimetry which directly determines the gravity vector.

As early as in the late sixties, when the inertial navigation system (INS) was first introduced for the survey purpose, its potential for recovering not only position, but also the anomalous gravity information was recognized (Nash, 1968; Huddle, 1977). It is interesting to note that the improvement of position accuracy is limited by the unknown anomalous gravity and system errors while, conversely, the gravity field could be determined from the INS if the accurate kinematic position were known and system errors could be kept small. So the key to recover the gravity vector is to separate gravitational acceleration from kinematic acceleration and sensor errors. This can be achieved by introducing external information. One economic way is to bring the vehicle, with the INS mounted on it, to a complete stop periodically and thus to obtain zero velocity update (ZUPT). This method, known as the semi-kinematic method, has been claimed to be successful with land vehicles (Salychev, etc., 1994; Wang, J & Z. Gao, 1996). According to Huddle (1988), with a very high precision INS, an accuracy of about 0.5 arcsec can be achieved for the deflections of the vertical. However for the large area survey, especially for geophysical exploration, this approach is still inefficient and expensive. The early instrumental consideration combined with INS for the gravity determination was the radio navigation system, Loran-C (LaCoste, et al. 1982). The obtained gravity accuracy was poor because of the low rate and low accuracy of kinematic position and velocity measurements. The idea of combining purely inertial sensors, an INS and a gravity gradiometer to separate gravitational and kinematic accelerations was proposed by Moritz (1967). The main problem with this proposed combination are the high cost and the extremely high sensitivity of gradiometers, which can even sense changes in the local gravity field due to a nearby moving operator. For the past five years, research in the airborne gravimetry has been active due to the fact that the vehicle acceleration can now be determined with sufficient accuracy from GPS carrier phase and phase rate measurements. The airborne implementation is attractive because it is less expensive and requires minimum time with large area coverage. Tests and discussions (Colombo, 1991; Gleason, 1992; Jekeli, 1994, 1993; Knickmeyer, 1990; Schwarz, 1994,1991,1987; Salychev, 1995,1994) has indicated that such a combination of systems is capable to recover the gravity information if properly integrated.

1.2 Statement of the Problem

Airborne gravity system determines the gravity disturbance by differencing a time series of gyro-stabilized accelerometer specific force and a time series of GPS derived aircraft acceleration. The difference yields the sum of the gravity disturbance and system noise.

GPS is a satellite-based navigation system that provides accurate position and velocity information. If anomalous gravity field determination is the sole purpose of the survey and its error is to remain less than 1 mgal, the requirements on the horizontal and vertical position have to be known to 6m and 3m respectively (Knickmeyer, 1990). This does not pose a problem for GPS with a combination of code and carrier measurements even in the presence of cycle slips. For all three velocity components, an accuracy of about 10 cm/s is necessary. GPS allows the determination of velocity with an accuracy of several cm/s (Schwarz et al., 1989). As to accelerations, the observations have to be averaged, usually within 1--5 min. Then the requirement for accelerations is that the low frequency acceleration errors are not beyond $10^{-5} m/s^2$ (Kleusberg, et al., 1989), which could be met by phase observations of GPS. It should be noted that the above requirements on external information is based on the individual effect on the direct measurement of the gravity disturbance. For the occasion where only one type of information, e.g. position, is used for estimation, the required accuracy should be more stringent. To achieve this, differential measurements as well as some processing techniques have to be incorporated. In the proposed LN-93 strapdown gravity system, differential GPS measurements with Ashtech XII or Trimble 4000 receivers are supposed to be used.

For the stabilization of a direction under motion, in which the gravity is observed, the following systems could be used:(Hein, 1995) (i) Damped two-axes platform systems; (ii) Schuler-tuned three axes space system; (iii) Strapdown inertial navigation system. Differential GPS-derived attitude measurements which in principle, could be used too, do not show the required accuracy, at least at present. Results of airborne gravity survey, using modified sea/air gravimeters with a damped two-axes platform, in Greenland, Antarctica and Switzerland show that airborne gravimetry with an accuracy of 3 to 5 mgal and a resolution of 10 km wavelength or better is operational today (Brozena, 1992; Brozena and Peters, 1994; Forsberg and Kenyon, 1994). It has been pointed out that insufficient platform stabilization may be the major problem for the improvement of the airborne gravimeters. The newly developed airborne gravity systems use an INS either as a stabilizing mount for a separate gravimetric sensor, which corresponds to the above Schuler-tuned platform system (ii), or as the gravimetric sensor itself, which corresponds to the strapdown system (iii). An airborne gravity system based on the high-accuracy Russian-made ITC-2 platform system and Trimble 4000 SSE GPS receivers was tested in Canada in 1994. It has been shown that an accuracy of 1 mgal with a wavelength of 2-3 km can be expected over a profile length of 50 km, see Salychev et al. (1994) and Salychev (1995). The result is achieved in the area with relatively smooth variation of the gravity field. New developments in recent years make it possible for accurate optical gyros, like the ring laser gyro (RLG), to be applied in the inertial navigation systems.

These systems can be used in the strapdown mode for vector gravity exploration. The strapdown inertial system differs from the platform navigation system in that the strapdown system, unlike platform systems, does not have a physical platform, and the inertial sensors are fixed with respect to the vehicle body and as such measure vehicle angular rate and acceleration vector components. Therefore, in a strapdown mechanization, the sensor data in body frame are transformed into local level frame computationally and then fed to the navigation equation. The main advantage of using strapdown systems for airborne gravimetry is its smaller size, lower cost, less power consumption and operational flexibility compared to that of platform systems. Papers by Schwarz et al. (1991), Gleason (1992), Jekeli (1992) and Wei and Schwarz (1994), have investigated some of the principles and concepts of strapdown gravity systems. The LN-93 standard ring laser gyro inertial navigation unit is the fifth generation product of Litton Guidance and Control System Co. LN-93 is applicable to a broad spectrum of military application. In this report the LN-93 inertial system combined with GPS measurements as an airborne gravity system is explored. The objective is to answer whether the LN-93 strapdown airborne gravity system is suitable for airborne gravimetry and to determine the accuracy that this combined system could yield in an operational setting.

There are two types of survey in airborne gravimetry: one is called scalar gravimetry which only determines the magnitude of the gravity anomaly in the normal direction; the other is vector gravimetry where the complete anomalous gravity vector is determined, i.e. the deflection of the vertical as well as the gravity anomaly. The major concern here is the determination of the vertical deflection. The difficulty of extracting the gravity information from the time-synchronized series of INS and GPS measurements is due to the extremely small signal to noise ratio. Typically the gravity disturbance amplitude would be 30 mgal and not exceed 100 mgal over distance of about 100 km (Hammada, 1995). A spectral method is used to characterize the anomalous gravity vector and compare it to the total error spectrum of airborne gravimetry systems. That part of spectral band in which the gravity signal is larger than the system noise will be called the spectral window of airborne gravimetry (Schwarz, 1995). Different filtering approaches now commonly used, known as Kalman filtering and wave estimation, are discussed in this report, and compared based on the system simulations.

2 SYSTEM DYNAMIC MODEL

2.1 General Principle of Airborne Gravimetry

The fundamental equation for gravity vector determination is based on Newton's second law of motion expressed in a non-rotating, freely falling coordinate frame, called the i-frame:

$$\ddot{x}^i = f^i + g^i \tag{2.1}$$

where $\ddot{x}$ is the second time derivative of the position vector; f is the specific force sensed by accelerometers and g is the gravitational acceleration. The inertial system comprises three mutually orthogonal accelerometers whose directions with respect to inertial space are defined by three gyros. The accelerometers do not sense gravitation g, as seen from equation (2.1), but accelerations derived from GPS include the gravitational effects. The problem is one of extracting the gravitation from a mix of two measurement systems (INS and GPS).

Transformed to the north-east-down (NED) local-level frame, called n-frame, (1.1) yields the following equation

$$\dot{v}^n = f^n - (\Omega_{en}^n + 2\Omega_{ie}^n)v^n + g^n - \Omega_{ie}^n \Omega_{ie}^n x^n \tag{2.2}$$

where v^n is the vehicle velocity vector with respect to the earth coordinatized in the n-frame; Ω_{en}^n and Ω_{ie}^n are the skew-symmetric matrices containing the angular velocity ω_{en}^n and ω_{ie}^n. ω_{en}^n is the angular velocity of the n-frame rotation with respect to an earth-fixed Cartesian frame; ω_{ie}^n is the angular velocity of Earth rotation with respect to the inertial frame, i-frame. The last two terms are respectively the gravitational vector and the centrifugal acceleration due to Earth's rotation, coordinatized in the n-frame. They can be together defined as the gravity vector $\bar{g}^n$, which can also be considered as the sum of the normal gravity vector γ^n and anomalous gravity vector δg^n. Therefore, omitting the superscript n, the three components of δg^n can be expressed as

$$\delta g_N = \dot{v}_N - f_N + (2\omega_e \cos\varphi + \frac{v_E}{R_p})v_E \tan\varphi - \frac{v_D v_N}{R_q} - \gamma_N \tag{2.3}$$

$$\delta g_E = \dot{v}_E - f_E - (2\omega_e \cos\varphi + \frac{v_E}{R_p})(v_D + v_N \tan\varphi) - \gamma_E \tag{2.4}$$

$$\delta g_D = \dot{v}_D - f_D + \frac{v_N^2}{R_q} + (2\omega_e \cos\varphi + \frac{v_E}{R_p})v_E - \gamma_D \tag{2.5}$$

where ω_e is the earth rotation rate; R_p and R_q are the radii of curvature in ellipsoidal meridian and prime vertical respectively; φ is the geodetic latitude; The subscripts N, E, D correspond to the three components in the NED local level frame.

From equations (2.3)--(2.5), it has been shown that the anomalous gravity vector can be determined by combining measurements from two hybrid systems, i.e. INS and GPS, as long as they are reasonably accurate enough, see Knickmeyer (1990) and Jekeli (1994).

2.2 Errors Affecting Airborne Gravimetry

In the INS/GPS based airborne gravimetry, the INS is designated to provide the specific force information in equations (2.3)--(2.5), and GPS is used to measure the position, velocity and acceleration of the aircraft using differential GPS processing techniques. In order to achieve the required kinematic accuracy, GPS measurements have to be recalculated to the center of the inertial unit (Salychev, 1995). This can be done by using INS attitude outputs.

By taking into account the individual error of all parameters included in equation (2.2), the significant errors affecting airborne gravimetry can be expressed as follows

$$\Delta\delta g = b_a + S_a f + C_a + W_a + \Psi f + \delta\dot{v}_G + D_t \tag{2.6}$$

where b_a is the bias of accelerometers;

$S_a = \begin{pmatrix} S_{a_N} & 0 & 0 \\ 0 & S_{a_E} & 0 \\ 0 & 0 & S_{a_D} \end{pmatrix}$, S_{a_N,a_E,a_D} indicate three accelerometer scale factors in n-frame.

C_a is the correlated noise of accelerometers. $\dot{C}_a = -\beta C_a + W_c$

β is the correlated coefficient; W_a, and W_c represent white noise

$\Psi = \begin{pmatrix} 0 & -\psi_D & \psi_E \\ \psi_D & 0 & -\psi_N \\ -\psi_E & \psi_N & 0 \end{pmatrix}$, $\psi_{N,E,D}$ are INS platform errors with respect to n-frame axes.

$\delta\dot{v}_G$ is the- GPS derived acceleration error.

D_t is the time synchronization error.

The first five items on the left side of equation (2.6) are the INS-related acceleration errors, which can be called specific force errors; the rest are GPS-related errors. Eventually the constant accelerometer bias has no effect on the estimation of gravity change and can be ruled out for the consideration here. Scale factor errors (including some nonorthogonal installation errors, which are not shown in the above equation) are usually compensated using laboratory tests or calibrated by some separate test runs and procedures (Schwarz, 1984). The INS platform (attitude) errors change slowly and are estimable with sufficient accuracy over a period of time. The random noise and GPS-derived acceleration errors can be smoothed to a low value in the frequency range of interest. As to the time synchronization errors, in the frequent band of interest, say $\omega \leq 2\pi / 60$ (1/sec), the acceptable time synchronization error would be 0.05 sec according to Salychev (1995). This is not a stringent requirement for dual-frequency GPS phase measurements. Some other long wavelength errors, like ionospheric delays and GPS orbit errors, are assumed to cancel in the process of estimating the acceleration and therefore are not considered here.

No matter what necessary procedures have to be taken, the major approach is to apply filtering technique in the estimation process. In this situation, the system dynamic model, as well as the observation model, is of much concern.

2.3 INS System Error Model

As LN-93 is a typical strapdown inertial system, its accelerometer output is the inertial acceleration of the vehicle and it is coordinatized in the body frame, called b-frame. The sensed specific force has to be transformed into local level n-frame in order to perform the navigation algorithm. The transformation matrix from the body frame to the n-frame is given by

$$C_b^n = R_3(-\alpha)R_2(-\chi)R_1(-\theta) \tag{2.7}$$

where θ, χ, α are the roll, pitch and yaw angles respectively; $R_j(\alpha)$ represents the rotation matrix about j-th axis by the angle α. The roll, pitch and yaw angles can be obtained by the following differential equation.

$$\begin{pmatrix} \dot{\theta} \\ \dot{\chi} \\ \dot{\alpha} \end{pmatrix} = \begin{pmatrix} 1 & \sin\theta\tan\chi & \cos\theta\tan\chi \\ 0 & \cos\theta & -\sin\theta \\ 0 & \sin\theta\sec\chi & \cos\theta\sec\chi \end{pmatrix} \omega_{nb}^b \tag{2.8}$$

where ω_{nb}^b indicates the angular rate of body frame with respect to n-frame coordinatized in the b-frame and it can be obtained from the gyro-sensed rates, ω_{ib}^b, and the computed rates, ω_{in}^n, as follows

$$\omega_{nb}^b = \omega_{ib}^b - C_n^b\omega_{in}^n \tag{2.9}$$

It is clear that after the transformation the same navigation equation (2.2) can be implemented in the strapdown mechanization. The only difference between the strapdown and the local-level stabilized system lies in the way of the transformation. With the strapdown mechanization, the transformation is done computationally using equation (2.7). In the local-level stabilized mode, the transformation is fulfilled mechanically through gyros, servos and related electronics. In both cases the Schuler feedback loop is the same and therefore the effect of errors associated with the gyros and accelerometers are essentially similar (however special orientation has to be taken into account for the sensors in a particular acceleration environment to minimize the systematic errors). Thus all the analysis of system dynamics in the local-level INS can also be applied to that of strapdown INS.

The underlying airborne gravity system is an INS system with a precise position update of GPS system assuming both INS system noise and GPS measurement noise are Gauss-Markov process or white noise. Considering only dominant terms as in equation 2.6, the accelerometer errors are modeled as a sum of constant bias, scale factor error and white noise. The gyro drift model only contains bias and white noise as the scale factor error is relatively small and negligible. The anomalous gravity model can be reasonably regarded as a 3rd order Markov process. Then by perturbating the navigation equation (2.2) (note: the perturbation of specific force includes orientation errors), the system model can be finally expressed by a set of linear first-order differential equations:

$$\dot{X} = FX + GW \tag{2.10}$$

where X is the state error vector; F is the dynamics matrix; G is the noise weight matrix and W represents white noise vector, $E[W(t)W(\tau)^T] = q\delta(t-\tau)$; q, the PSD of white noise, is a constant; $\delta(t-\tau)$ is a delta function.

For the convenience of investigation, the state vector X can be partitioned into three vectors of lower dimensions:

$$X = \begin{bmatrix} X_1 & X_2 & X_3 \end{bmatrix}^T \tag{2.11}$$

The error state X_1 describes the behavior of the orientation, velocity and position errors of the inertial system with respect to local NED frame; X_2 is used to model the sensor errors, i.e. accelerometers errors, and gyros drift; while X_3 is the states associated with the 3rd-order Gauss-Markov models for the three gravity disturbance components. To be specific, we have

$$X_1 = \begin{pmatrix} \psi_N & \psi_E & \psi_D & \delta v_N & \delta v_E & \delta v_D & \delta\varphi & \delta\lambda & \delta h_D \end{pmatrix}^T \tag{2.12}$$

$$X_2 = \begin{pmatrix} b_{\varepsilon_N} & b_{\varepsilon_E} & b_{\varepsilon_D} & b_{a_N} & b_{a_E} & b_{a_D} & S_{a_N} & S_{a_E} & S_{a_D} \end{pmatrix}^T \tag{2.13}$$

$$X_3 = \begin{pmatrix} \delta g_N & \delta g_E & \delta g_D & \delta g_N' & \delta g_E' & \delta g_D' & \delta g_N'' & \delta g_E'' & \delta g_D'' \end{pmatrix}^T \tag{2.14}$$

where $\delta v_{N,E,D}$ are velocity errors expressed in n-frame; $\delta\varphi$, $\delta\lambda$, δh_D represent latitude, longitude and down-pointed height errors respectively; $b_{\varepsilon_N,\varepsilon_E,\varepsilon_D}$ are gyro drifts with respect to n-frame; $\delta g_N, \delta g_E, \delta g_D$ denote three components of the anomalous gravity in the local level n-frame. Therefore according to the system dynamics in local level frame, the total system state equations can be rewritten as

$$\frac{d}{dt}\begin{bmatrix} X_1 \\ X_2 \\ X_3 \end{bmatrix} = \begin{bmatrix} F_{11} & F_{12} & F_{13} \\ 0 & 0 & 0 \\ 0 & 0 & F_{33} \end{bmatrix}\begin{bmatrix} X_1 \\ X_2 \\ X_3 \end{bmatrix} + G\begin{bmatrix} W_1 \\ W_2 \\ W_3 \end{bmatrix} \tag{2.15}$$

where

$$F_{11} = \begin{bmatrix} 0 & -l\sin\varphi & \dot{\varphi} & 0 & 1/R & 0 & -l\sin\varphi & 0 & 0 \\ l\sin\varphi & 0 & l\cos\varphi & -1/R & 0 & 0 & 0 & 0 & 0 \\ -\dot{\varphi} & -l\cos\varphi & 0 & 0 & -tg\varphi/R & 0 & -l\cos\varphi & 0 & 0 \\ 0 & -f_D & f_E & 0 & -2l\sin\varphi & 2\dot{\varphi} & -llR\cos2\varphi & 0 & [\ddot{\varphi}+\frac{1}{2}ll\sin2\varphi] \\ f_D & 0 & -f_N & 2l\sin\varphi & 0 & 2l\cos\varphi & (2l\dot{\varphi}+\ddot{\lambda}tg\varphi)/R\cos\varphi & 0 & (\ddot{\lambda}-2l\dot{\varphi}tg\varphi)\cos\varphi \\ -f_E & f_N & 0 & -2\dot{\varphi} & -2l\cos\varphi & 0 & -Rll\sin2\varphi & 0 & \dot{\varphi}^2+2\omega_s^2+ll\cos\varphi^2 \\ 0 & 0 & 0 & 1/R & 0 & 0 & 0 & 0 & 0 \\ 0 & 0 & 0 & 0 & 1/R\cos\varphi & 0 & 0 & 0 & 0 \\ 0 & 0 & 0 & 0 & 0 & 1 & 0 & 0 & 0 \end{bmatrix}$$

$$F_{12} = \begin{bmatrix} 1 & 0 & 0 & 0 & 0 & 0 & 0 & 0 & 0 \\ 0 & 1 & 0 & 0 & 0 & 0 & 0 & 0 & 0 \\ 0 & 0 & 1 & 0 & 0 & 0 & 0 & 0 & 0 \\ 0 & 0 & 0 & 1 & 0 & 0 & f_N & 0 & 0 \\ 0 & 0 & 0 & 0 & 1 & 0 & 0 & f_E & 0 \\ 0 & 0 & 0 & 0 & 0 & 1 & 0 & 0 & f_D \\ 0 & 0 & 0 & 0 & 0 & 0 & 0 & 0 & 0 \\ 0 & 0 & 0 & 0 & 0 & 0 & 0 & 0 & 0 \\ 0 & 0 & 0 & 0 & 0 & 0 & 0 & 0 & 0 \end{bmatrix}$$

$$F_{13} = \begin{bmatrix} 0 & 0 & 0 & 0 & 0 & 0 & 0 & 0 & 0 \\ 0 & 0 & 0 & 0 & 0 & 0 & 0 & 0 & 0 \\ 0 & 0 & 0 & 0 & 0 & 0 & 0 & 0 & 0 \\ 1 & 0 & 0 & 0 & 0 & 0 & 0 & 0 & 0 \\ 0 & 1 & 0 & 0 & 0 & 0 & 0 & 0 & 0 \\ 0 & 0 & 1 & 0 & 0 & 0 & 0 & 0 & 0 \\ 0 & 0 & 0 & 0 & 0 & 0 & 0 & 0 & 0 \\ 0 & 0 & 0 & 0 & 0 & 0 & 0 & 0 & 0 \\ 0 & 0 & 0 & 0 & 0 & 0 & 0 & 0 & 0 \end{bmatrix}$$

$$F_{33} = \begin{bmatrix} 0 & 0 & 0 & 1 & 0 & 0 & 0 & 0 & 0 \\ 0 & 0 & 0 & 0 & 1 & 0 & 0 & 0 & 0 \\ 0 & 0 & 0 & 0 & 0 & 1 & 0 & 0 & 0 \\ 0 & 0 & 0 & 0 & 0 & 0 & 1 & 0 & 0 \\ 0 & 0 & 0 & 0 & 0 & 0 & 0 & 1 & 0 \\ 0 & 0 & 0 & 0 & 0 & 0 & 0 & 0 & 1 \\ -\beta_1^3 & 0 & 0 & -3\beta_1^2 & 0 & 0 & -3\beta_1 & 0 & 0 \\ 0 & -\beta_2^3 & 0 & 0 & -3\beta_2^2 & 0 & 0 & -3\beta_2 & 0 \\ 0 & 0 & -\beta_3^3 & 0 & 0 & -3\beta_3^2 & 0 & 0 & -3\beta_3 \end{bmatrix}$$

$l = \dot{\lambda} + \omega_e$, ω_e is the earth rotation rate; $ll = \dot{\lambda}(\dot{\lambda} + 2\omega_e)$; R is the earth radius, ω_s is the Schuler angular rate; $f_{N,E,D}$ indicate specific forces sensed by accelerometers in NED frame; $\beta_{1,2,3}$ are parameters for gravity model related to the correlation length.

2.4 GPS Observation Model

The general observation model can be written as

$$Z = HX + V \tag{2.16}$$

where Z is the observation vector; H is the observation matrix; V is the observation noise. $E[V(t)V(\tau)^T] = r\delta(t-\tau)$, r is the PSD of the observation noise.

The GPS serves the positioning and navigation communities very well. It has been demonstrated that the receiver position relative to known point of a base station can be determined to a precision of 1 cm (Wei et al, 1992). The feasibility of precise GPS positioning for airborne gravimetry has also been analyzed by Kleusberg et al. (1990) and Colombo (1992). In this simplified view of direct observations of the position errors, the observation matrix should be

$$H = \begin{bmatrix} \underset{3\times 6}{0} & \underset{3\times 3}{I} & \underset{3\times 18}{0} \end{bmatrix} \tag{2.17}$$

where I indicates unit matrix.

In many cases, the GPS-derived acceleration or velocity need to be known with high accuracy for gravimetry. Usually the GPS acceleration can be determined by differentiating the time series of the GPS positions twice in time(Brozena et al., 1989). Jekeli (1994b), and Jekeli and Garcia. (1996) proposed an alternative of deriving acceleration from the GPS signal by directly differentiating the carrier phase. The advantage of using phase directly is that the second time derivative of the phase, being a truer form of an acceleration determined by GPS, is generally transparent to cycle slips, phase offsets, full-cycle ambiguity and to some extent also satellite and receiver clock errors.

3 THE SPECTRAL WINDOW OF AIRBORNE GRAVIMETRY

The concept of the spectral window of airborne gravimetry comes from Schwarz etc. (1994), where it was defined as a spectral range in which the gravity signal is larger than the system noise.

The feasibility of vector gravimetry using INS and GPS measurements has been widely studied in both time and frequency domains. By a covariance analysis Knickmeyer (1990) investigated the requirements on INS and GPS observations and compared the performance of different INS mechanization for gravity vector determination. She further concluded that a so-called medium accuracy INS could not be used for accurate gravimetry. However, if the power of the gravity signal is stronger than that of the estimation error at a certain frequency band, the gravity can be recovered for that range of frequencies. The concept of signal to error ratio was used, by Jekeli (1994), to analyze the gravity estimation performance of a combination of INS and GPS of different accuracy level. It is concluded that the horizontal components of gravity with wavelengths shorter than 250 km should be estimable to an accuracy of 4-6 mgal with medium accuracy INS/GPS (high accuracy accelerometer) systems and 1-2 mgal with high accuracy systems. Similarly, Schwarz etc. (1994) come to the conclusion by spectral analysis that, by state-of-the-art hardware, the spectral window should be between 15 km and 100 km in flat areas, and between 10 km and 200 km in mountainous areas. The objective of this section is to facilitate this discussion and to investigate the possibility of gravity recovery for an airborne LN-93 inertial system with the aid of GPS measurements, making use of available sources and techniques.

Generally, by combining measurements from both INS and GPS (see equations (2.3)--(2.5)), the gravity vector can be estimated as long as the measurements are accurate enough. The major function of the GPS subsystem in this situation is to provide a precise kinematic description of the vehicle trajectory. By current state of the art, GPS provides the position and velocity with sufficient accuracy according to Knickmeyer (1990). The critical factor in improving the performance of airborne gravimetry is the accuracy of GPS-derived kinematic acceleration. The total error turns out to be a combination of errors in specific force sensed by INS accelerometers and errors in kinematic acceleration derived from GPS.

3.1 Spectral Properties of the Gravity Field

The power spectral density (PSD) of the gravity field model can be obtained from known, densely distributed, point gravity data by some spectral estimation approaches like the fast Fourier transform (FFT), the maximum-likelihood method (MLM), the maximum-entropy method (MEM) and the auto-regressive method (AR). Reference goes to Kay (1988), and McLellan (1982). Or it can be approximated mathematically by certain processes or functions. As there is no dense point gravity data at hand, the latter approach is of major concern for the moment.

Two types of gravity covariance model are commonly used. One is so called the reciprocal distance model (Moritz, 1976; Jordan 1981). The other corresponds to the third-order Gauss-Markov process (Gelb, 1974). The gravity field is assumed to be isotropic and a stationary stochastic process. For the representation of the disturbance field using a reciprocal distance model, in its spherical coordinate form, the covariance function is (for disturbing potential, T)

$$C_{TT}(d,h) = \frac{\sigma^2}{[(1+\beta h)^2 + \beta^2 d^2]^{1/2}} \tag{3.1}$$

where σ^2, β are parameters with units of m^4/s^4 and $1/m$ respectively; d is the distance between two points in the horizontal plane; h is the sum of the height of the two points above the earth surface. According ιo Gradshteyn & Ryzhik. (1980), the corresponding power spectral density, the Fourier transform of the covariance function, is given by:

$$S_{TT}(\omega,h) = 2\pi\sigma^2 \frac{e^{-\omega(1/\beta+h)}}{\beta\omega} \tag{3.2}$$

where ω represents the frequency. The covariance function of the third-order Gauss-Markov process is:

$$C_{TT}(d) = \sigma^2 e^{-\beta d}(1+\beta d+\frac{1}{3}\beta^2 d^2) \tag{3.3}$$

Where the parameters σ^2, β have the same units as in equations (3.1) (3.2). Note that d is the distance between two points and the process described here is two-dimensional. The corresponding PSD can be obtained from two-dimensional Fourier Transformations:

$$S_{TT}(\omega) = 10\pi\sigma^2 \frac{\beta^5}{(\beta^2 + \omega^2)^{7/2}} \tag{3.4}$$

For the simplification of the discussion here, a one dimensional, along-track horizontal gravity signal was selected. The models chosen for the covariance function of the disturbing potential are linear combinations of two third-order Gauss-Markov processes of baseline gravitational signatures. The covariance function for the disturbing potential is then

$$C_T(d) = \sum_{i=1}^{2} \sigma_i^2 e^{-\beta_i d}(1 + \beta_i d + \frac{1}{3}\beta_i^2 d^2) \tag{3.5}$$

and the PSD of the horizontal gravity disturbance (derivative of T along one direction) is

$$S_{\delta g}(\omega) = \frac{16}{3}\omega^2 \sum_{i=1}^{2} \frac{\sigma_i^2 \beta_i^5}{(\omega^2 + \beta_i^2)^3} \tag{3.6}$$

where the parameters of two third-order Gauss-Markov processes for the baseline model are (Jekeli, 1995)

$\sigma_1^2 = 350 \quad m^4 / s^4$ $\qquad\qquad$ $\beta_1 = 1.4 \times 10^{-5}$ 1/m

$\sigma_2^2 = 80000 \quad m^4 / s^4$ $\qquad\qquad$ $\beta_2 = 1.0 \times 10^{-6}$ 1/m

It is assumed that the aircraft flies at constant speed of 360 km/hr. Thus the distance quantities, divided by velocity, can be converted to time. The power spectral density for the model is shown as in Figure 3.1.

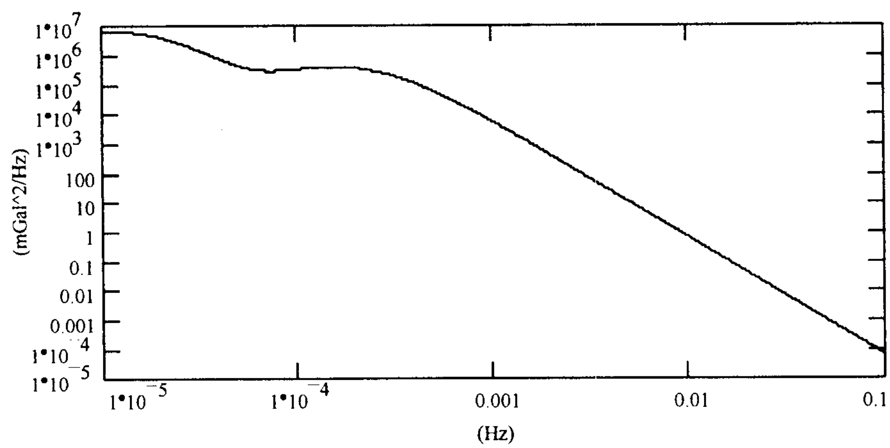

Fig. 3.1 The PSD of the gravity disturbance modeled by the third-order Gauss-Markov processes

3.2 Spectral Properties of the GPS-derived Acceleration Error

As stated in section 2.4, GPS acceleration can be either determined from GPS derived position by double differentiation (Schwarz et at., 1991), or achieved by directly differentiating the phase measurements. Since there is no specific process model available for the GPS to describe the characteristics of its derived acceleration error, the obtained differences between the heights sensed by laser altimeter and that by GPS could be taken as true GPS errors in order to examine the PSD of the GPS-derived acceleration error. The height data was collected during a flight test over Lake Ontario (Schwarz et al., 1994), where four Trimble 4000 SSE GPS receivers were used in C/A-code mode. A fifth-order polynomial function was chosen to fit the averaged PSD of the GPS derived acceleration errors.

$$S_{GPS} = p_5\omega^5 + p_4\omega^4 + p_3\omega^3 + p_2\omega^2 + p_1\omega + p_0 \tag{3.7}$$

where S_{GPS} is the PSD of the GPS-derived acceleration error; p_i $(i = 0...5)$ are the parameters. By making use of the obtained parameters, given in the following, the PSD log-log plot for GPS derived acceleration error is shown here, in Fig. 3.2, for the underlying analysis.

p_5=2.4701e8, p_4=3.1875e7, p_3=1.4767e6, p_2=-2.9591e4, p_1=3.5022e0, p_0=9.3150e-1

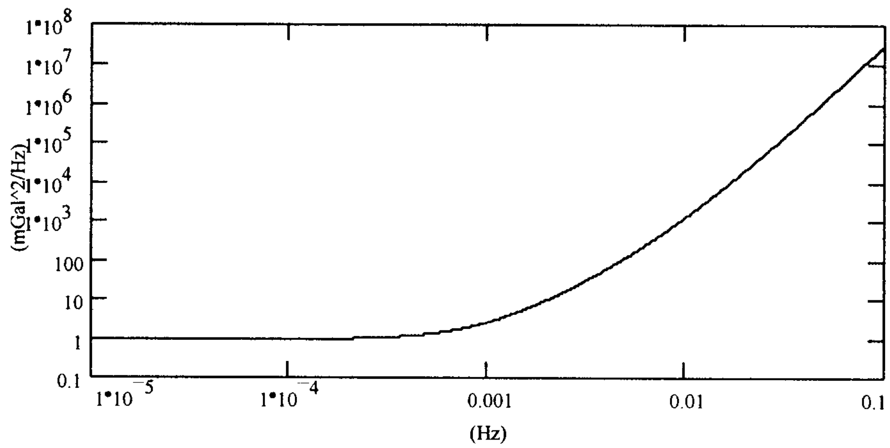

Fig. 3.2 The PSD of the GPS derived acceleration errors

From the figure one can see the GPS derived acceleration error is concentrated in the higher frequency range.

3.3 Spectral Properties of the LN-93 Accelerometer Error

According to the system specification, the essential error budget of LN-93 inertial system is listed in Table 3.1 (Litton, 1985).

It is well known that the spectrum of the specific force error is concentrated at the low end of the spectrum in airborne gravimetry while GPS noise dominates the high frequency part of the spectrum. From equation (2.6) we know that the acceleration error sensed by INS accelerometers, i.e. specific force error, generally consists of five parts. They are accelerometer biases, scale factor errors, platform misalignment errors, colored noise and white noise. Scale factor errors or non-orthogonality errors usually do not

	Accelerometer	Gyro
Bias repeatability	15 ug	0.003 deg/hr
Scale factor error	120 ppm	5 ppm
Correlated noise	2 ug, 5min correlation time	0.002 deg/hr, 10 min cor. time
white noise	10ug/$\sqrt{Hz}$	0.001 deg/hr/$\sqrt{Hz}$

Table 3.1 Essential error budget for LN-93 system

change from time to time and can be kept small by special calibrations. Their effects are omitted for the present consideration. The constant accelerometer bias, with its spectrum being delta function $\delta(\omega)$, will cause the platform to oscillate at Schuler frequency ω_s. and have no effects on the overall error spectrum except at ω_s, where the spectral power tends to be infinite. So the PSD of the INS specific force includes three parts: white noise, colored noise, of accelerometers, and the acceleration error induced by attitude errors. For white noise, and colored noise being considered as a 1st-order Gauss-Markov process, their PSD can be simply written out respectively as

$$S_{W_a} = Q_a^{\ 2} \tag{3.8}$$

$$S_{W_c} = \frac{2\beta_a}{\omega^2 + \beta_a^{\ 2}} \sigma_a^{\ 2} \tag{3.9}$$

where $Q_a^{\ 2}$ is the PSD of white noise; σ_a^2 is the variance of accelerometer colored noise; β_a is the inverse of the correlation time of the accelerometer correlated noise.

As to the acceleration error induced by attitude errors, the spectral analysis is rather complicated. To derive its PSD, we first have to know some facts about the linear system with random inputs. Any linear differential equations can be figured as a transfer function with the inputs and the output as well as the initial conditions, see Figure 3.3. The output

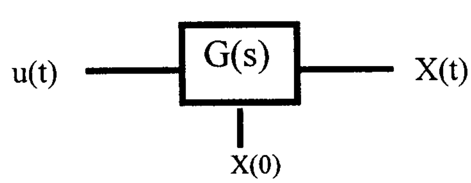

u(t)=Input
X(t)=Output
X(0)=Initial condition
G(s)=X(s)/u(s),
=Transfer function

Fig. 3.3 Block diagram of linear systems

solution consists of two parts, i.e. homogeneous solution and particular solution. The homogeneous solution is related to the initial condition and mainly reveals a harmonic oscillator with Schuler frequency for inertial system. This solution is of no interest to our discussion here. Assuming that the transfer function G(s) in Fig. 3.3 represents a stable , fixed-parameter system and that the input is stationary with a known spectral function, according to Brown (1983), the equation relating the input and output spectral functions is

$$S_x(\omega) = |G(j\omega)|^2 S_u(\omega) \tag{3.10}$$

Here the major input error source includes accelerometer errors a, gyro drifts ε and gravity disturbances δg while the output is attitude error ψ. Based on the system error dynamics in section 2.3, the Laplace transform of the attitude should be (consider only the east accelerometer channel.)

$$\psi(s) = -\frac{1}{R(s^2+\omega_s^{\ 2})}(a(s)+\delta g(s)) + \frac{s^3}{(s^2+\omega_s^{\ 2})(s^2+\omega_e^{\ 2})}\varepsilon(s) \tag{3.11}$$

Therefore, using equation (3.10), the spectral function of the attitude-induced acceleration error turns out to be

$$S_{\psi g}(\omega) = \frac{\omega_s^{\ 4}}{(\omega^2-\omega_s^{\ 2})^2}(S_a(\omega)+S_{\delta g}(\omega)) + \frac{\omega^6 g^2}{(\omega^2-\omega_s^{\ 2})^2(\omega^2-\omega_e^{\ 2})^2}S_\varepsilon(\omega) \tag{3.12}$$

where the subscript ψg indicates the product of attitude error and gravity value. Since the constant bias does not generate any spectral power except at $\omega = 0$, we only consider the influence of white noise and colored noise of the accelerometer and the gyro. The colored noise is viewed as a first-order Gauss-Markov process. Then we have

$$S_a(\omega) = Q_a^{\ 2} + \frac{2\beta_a\sigma_a^{\ 2}}{\omega^2+\beta_a^{\ 2}} \tag{3.13}$$

$$S_\varepsilon(\omega) = Q_\varepsilon^{\ 2} + \frac{2\beta_\varepsilon\sigma_\varepsilon^{\ 2}}{\omega^2+\beta_\varepsilon^{\ 2}} \tag{3.14}$$

where $Q_\varepsilon^{\ 2}$ is the PSD of gyro white noise and σ_ε^2, β_ε are the variance and the inverse of correlation time, respectively, of gyro colored noise. The spectral function of the gravity disturbance, $S_{\delta g}$, is given by equation (3.6). Thus by adding up equations (3.8), (3.9) and (3.12), and making use of equations (3.6), (3.13) and (3.14), the PSD of specific force error of LN-93 inertial system is shown in Fig. 3.4.

The two spikes shown in Fig. 3.4 occur at the frequencies of Schuler and Earth-rate which are the poles of the system transfer function. The spikes can be interpreted as follows: at the Schuler and Earth-rate frequencies, the system error input will resonate with the system natural frequency and thus the spectral power there will reveal a characteristic of infinity. They also indicate that at the mentioned two frequencies the gravity information is indistinguishable from system errors.

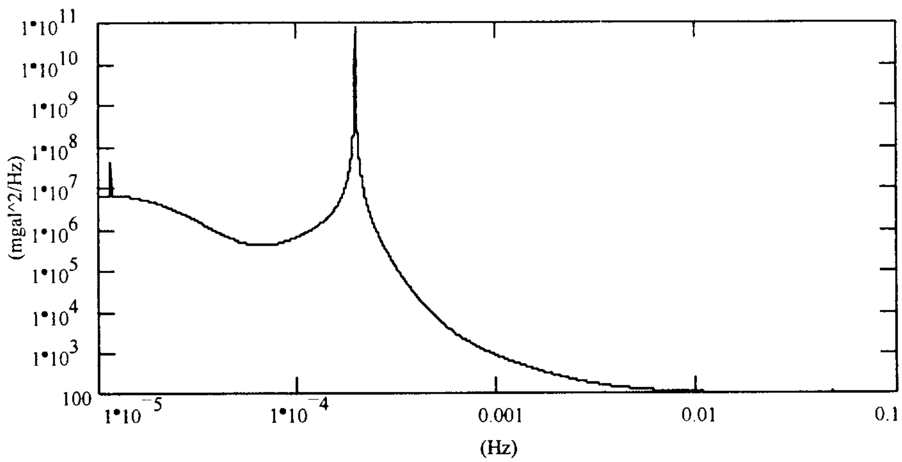

Fig. 3.4 The PSD of the specific force error of the LN-93 inertial system

3.4 Spectral properties of the Total Acceleration Error Compared with That of the Gravity Model

Obviously the PSD of the total error source for the determination of gravity vector is the arithmetic sum of the INS and GPS acceleration errors, as shown in Figure 3.5, because these two effects are mutually uncorrelated.

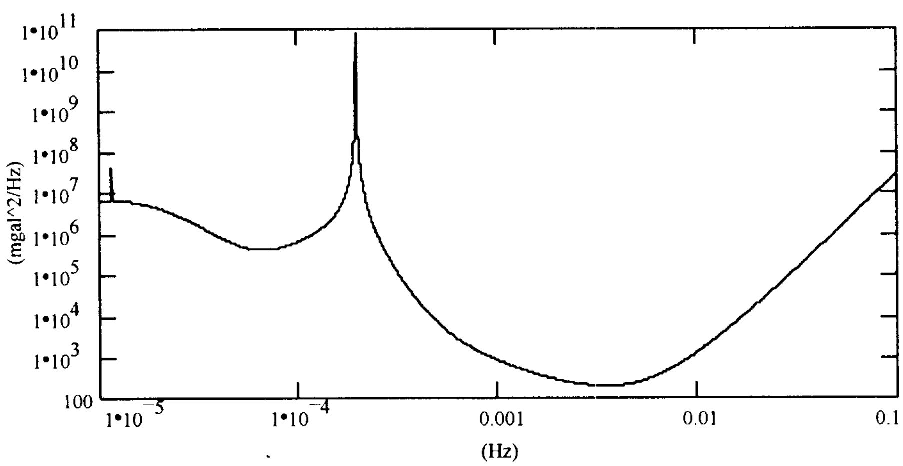

Fig. 3.5 The PSD of the total INS/GPS acceleration error

For comparison, the PSD of gravity disturbance and that of the combined GPS/INS acceleration error are both given in the same chart as in Figure 3.6. As we already know, the gravity disturbance is estimable when the useful signal is greater than system noise. From the figure one can see that the said integrated INS (LN-93)/GPS system is able to recover the anomalous gravity vector information at the frequency band of 2.99×10^{-4} Hz~2.23×10^{-3} Hz, i.e. the wavelength from 45 km to 334 km, with regard to the baseline gravity signature.

In the Earth, different areas, like flat area and mountainous area, have different gravitational signatures, and thus would yield different spectral windows for airborne gravimetry. So would the different altitudes. However, here we assume the mission is performed at the same height and the altitude factor is ignored for the present discussion. The parameters for the three types of gravity signature are listed in Table 3.2 (Jekeli, 1995).

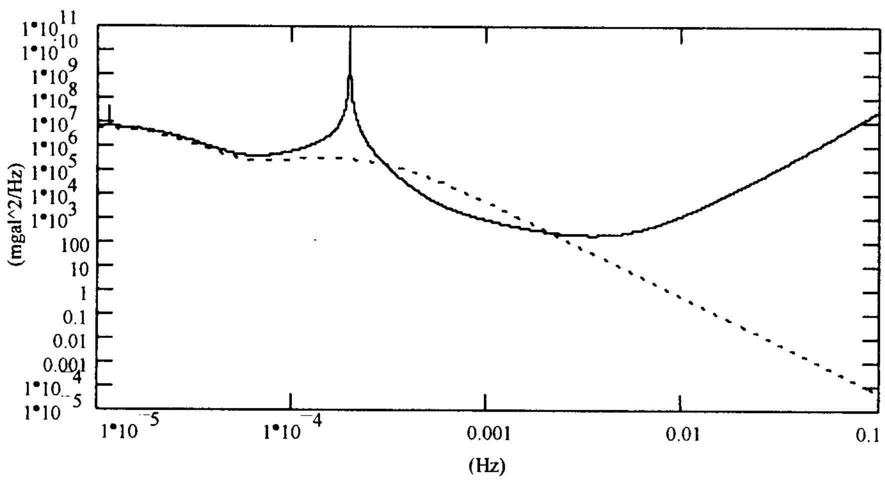

Fig. 3.6 The PSD of the gravity disturbance and the combined GPS/INS acceleration errors

Model	$\sigma_i^2[m^4/s^4]$	$\beta_i[1/m]$
Rough	1000 80000	2.5×10^{-5} 1.0×10^{-6}
Baseline	350 80000	1.4×10^{-5} 1.0×10^{-6}
Smooth	200 80000	0.9×10^{-5} 8.5×10^{-7}

Table 3.2 Parameters of the different gravity models

The vehicle speed is still 360 km/hr. The spectral properties for airborne gravimetry with these three types of gravity signatures are put together in Figure 3.7 in terms of the signal-to-noise ratio, i.e.,

$$\gamma(\omega) = \sqrt{\frac{S_{\delta g}(\omega)}{S_{sp}(\omega) + S_{GPS}(\omega)}} \tag{3.15}$$

Where the sum of the PSD of the specific force PSD, $S_{sp}(\omega)$, and that of the GPS-drived acceleration error, $S_{GPS}(\omega)$, represents the system noise spectrum. The corresponding spectral windows for different cases are summarized in Table 3.3.

In the practical implementation, the operational spectral window will change with the vehicle speed. For the comparative study, we investigate the lower speed situation, say, road tests using a van. The vehicle speed is assumed 80 km/hr here. Similarly using the signal-to-noise ratio we get the spectral properties for road tests, as shown in Figure 3.8, with summarized results in Table 3.4.

Gravity Model	Frequency range [Hz]	Wavelength [km]
Rough	$2.95 \times 10^{-4} \sim 5.73 \times 10^{-3}$	17~338
Baseline	$2.99 \times 10^{-4} \sim 2.23 \times 10^{-3}$	45~334
Smooth	None	None

Table 3.3 The spectral windows for airborne gravimetry with different gravity signatures

Gravity Model	Frequency range [Hz]	Wavelength [km]
Rough	$2.85 \times 10^{-4} \sim 1.92 \times 10^{-3}$	12~81
Baseline	None	None
Smooth	None	None

Table 3.4 The spectral windows for road tests with different gravity signatures

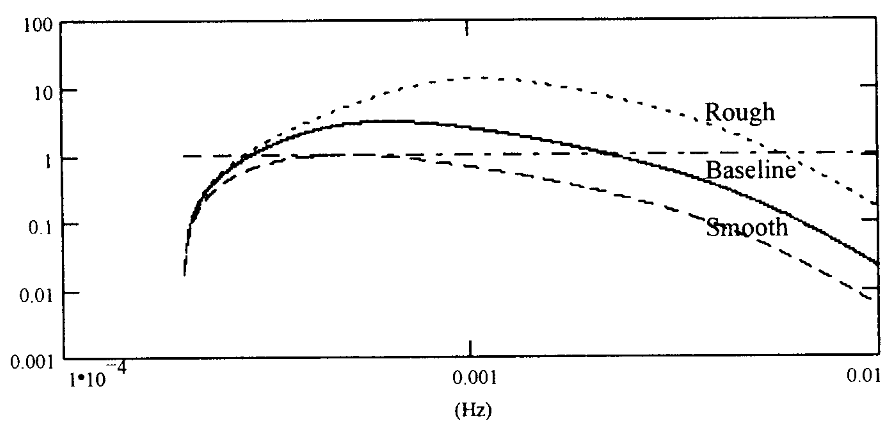

Fig. 3.7 The signal-to-noise ratio with different gravity signatures (v=360km/hr)

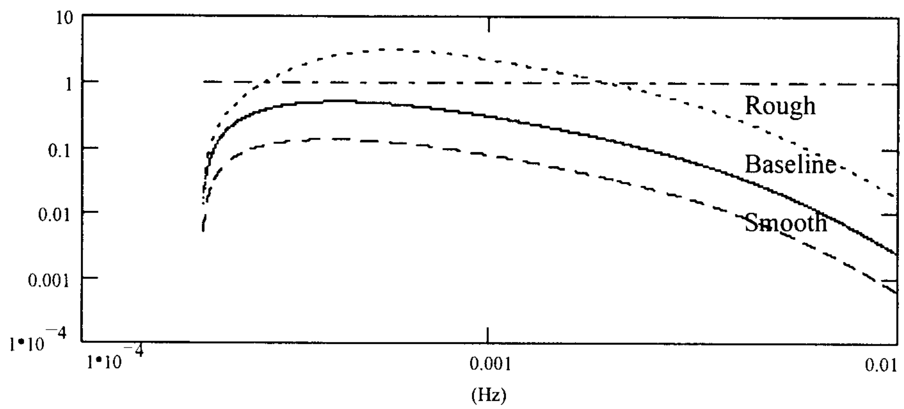

Fig. 3.8 The signal-to-noise ratio with different gravity signatures (v=80km/hr)

From the above discussion, one can find that LN-93 strapdown system supplemented with high accuracy GPS measurements is suitable for vector gravimetry, especially at the medium wavelength with the sufficient variation of gravity (rough and baseline gravity signature). Generally the estimable spectral window is larger for mountainous areas than for flat areas. As to the road test of lower speed, the gravity disturbance signal is only recoverable for the rough gravity model, as seen from Figure 3.8.

3.5 Further discussions based on the contribution of different error sources

By exploring the PSD of the specific force error, we have shown that it is mainly caused by three error sources: accelerometer errors, gyro drifts and gravity disturbances. Their influence are all concentrated at the low end of the spectrum in airborne gravimetry. However for each individual error source its effect differs from one another. The gravity disturbance, being a desired signal, is one of the major error sources to the system attitude as well. The spectral properties of three error sources induced acceleration error with rough and baseline gravity fields are given in Fig. 3.9 and Fig. 3.10 respectively.

It can be seen, from the Figures 3.9 and 3.10, that the acceleration error induced by the gravity disturbance dominates the lower part of the interested frequency range while that induced by the accelerometer and the gyro do the higher part. So the demonstrated features indicate that the gravity disturbance, as an error source, will primarily influence the long wavelength performance of airborne gravimetry. This conclusion will be verified in the following system simulation.

Similarly, the specific force error here can be regarded as two components: One is directly related to the accelerometer sensor error, being a combination of white noise and colored noise; The other is the attitude-induced acceleration error due to the system errors. To investigate and compare their difference will help find an effective approach to improve the performance for airborne gravimetry. Fig 3.11 shows the different error contribution due to the accelerometer sensor and the attitude error. It has been shown that the PSD of attitude-induced acceleration error is larger than that of the accelerometer noise for most part of estimable frequency range. Therefore one can conclude from this analysis that, in order to improve the gravity estimability significantly, the improvement should be made to reduce the attitude error, e.g., to introduce the external attitude information, like, from photogrammetry.

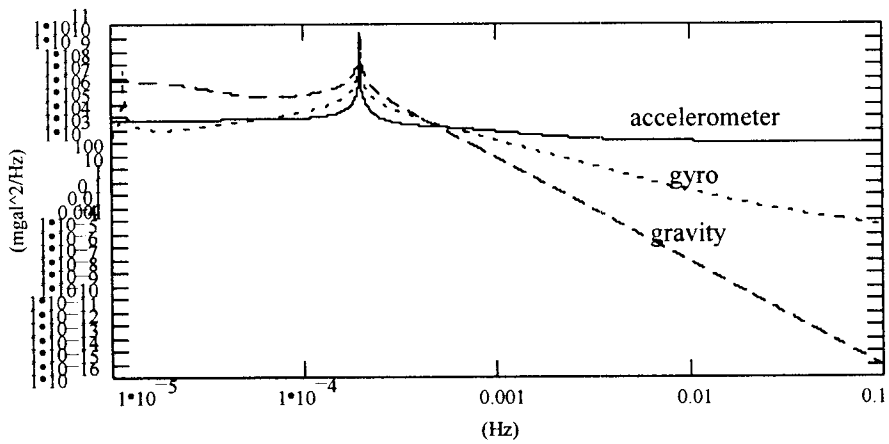

Fig. 3.9 The spectral properties of acceleration errors due to the accelerometer, the gyro and the gravity disturbance (baseline) respectively

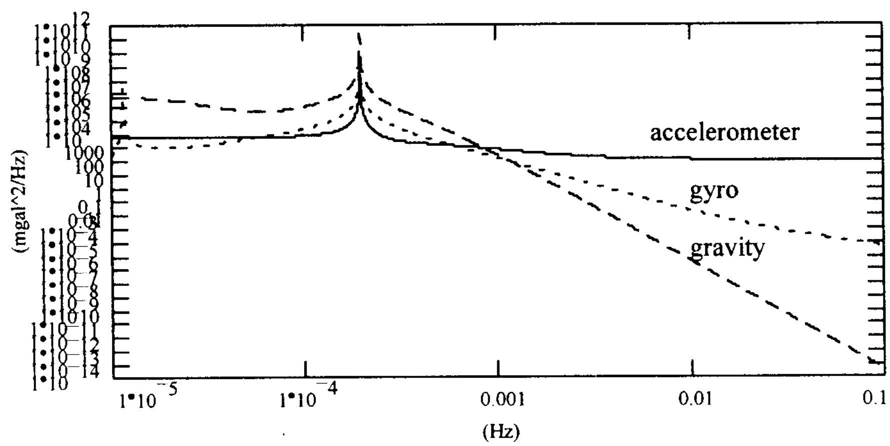

Fig. 3.10 The spectral properties of acceleration errors due to the accelerometer, the gyro and the gravity disturbance (tough) respectively

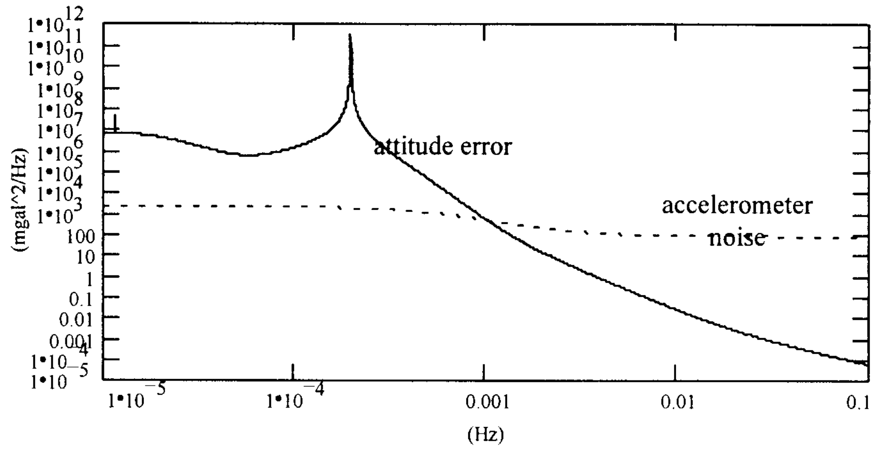

Fig. 3.11 The spectral properties of acceleration errors due to the accelerometer noise and the attitude error

4 ESTIMATION METHODS

As stated in section 2.1 the measurements from both INS and GPS systems are affected by large noise with different frequency components. The challenge is to develop the appropriate estimation approaches to recover the useful signal from the noisy measurement. Basically two different approaches are commonly used in airborne gravimetry. They are Kalman filtering and wave estimation.

4.1 Discrete Kalman-Bucy Filtering

The conventional Kalman filter is well known (Gelb, 1974; Anderson and Moore, 1979). It calculates recursively forward and estimates state errors constantly. With the system and observation model given, as in section 2, the discrete estimating equations, known as Kalman-Bucy filter, are given as follows:

From (2.6) and(2.12), we first take their discrete form

$$X_k = \Phi_{k,k-1} X_{k-1} + G_{k-1} W_{k-1} \tag{4.1}$$

$$Z_k = HX_k + V_k \tag{4.2}$$

Assuming the interval $\Delta t = t_k - t_{k-1}$ is short, so approximation could be made as

$$\Phi_{k,k-1} \approx I + F(t_{k-1})\Delta t + \frac{1}{2!} F(t_{k-1})\Delta t^2 \tag{4.3}$$

$$G_k \approx G(t_k) \tag{4.4}$$

$$W_k \approx \int_{t_{k-1}}^{t_k} W(t)dt \tag{4.5}$$

where $E[V_k V_k^T] = r_k$ and $E(W_k W_k^T) = q\Delta t = Q_k$

Then we have following estimate equations.

Time propagation equations:

$$\begin{aligned} \hat{X}_k^- &= \Phi_{k,k-1} \hat{X}_{k-1}^+ \\ P_k^- &= \Phi_{k,k-1} P_{k-1}^+ \Phi_{k,k-1}^T + G_{k-1} Q_{k-1} G_{k-1}^T \end{aligned} \tag{4.6}$$

Observation update equations:

$$\hat{X}_k^{+} = \hat{X}_{k-1}^{-} + K_k \rho_k$$
$$P_k^{+} = (I - K_k H) P_k^{-} \tag{4.7}$$

where P_k is the estimated covariance; $\rho_k = Z_k - H\hat{X}_k^{-}$ is innovation; $K_k = P_k^{-} H^T D_k^{-1}$ denotes Kalman gain and $D_k = HP_k^{-} H^T + r_k$ indicates predicted residual covariance.

Sometimes the optimal smoother is required to be applied for better estimation results. In principle, the smoothing goes forward then backward in time, performing a Kalman-like recursion, where the filtered states and their covariances do not have to be saved, except at the point at which the smoothed estimate is desired. One of the most popular smoothing algorithm is called modified Bryson-Frazier (mBF) (Bierman, 1973).

In the above we considered the system noise W and the measurement noise V to be uncorrelated. However in airborne gravimetry, depending on how the system model and observation model are formed (like the deterministic model below), the two kind of noises are often correlated with themselves. If a system noise is colored, one can simply use shaping filter to change it into a white noise. If a measurement noise is correlated with itself or even with a system noise, the above Kalman recursive equations have to be modified to accommodate this situation. The reference is made to Brown (1983)

4.2 Wave Estimation

In wave estimation, a deterministic system error model representation of INS is used. Such an approach assumes that input disturbances acting on the system are not described by random processes but by a deterministic function (within a certain time interval) of unknown intensity which can be estimated. The main idea and general procedure for the wave approach is presented in the following.

4.2.1 Intuitive Concept of Wave Estimation

According to Salychev (1995) and Salychev et al. (1995), the whole mission time is divided into a series of small estimation cycles. In each cycle, the input disturbance is described by a linear combination of known base functions with unknown coefficients, instead of statistical noise

$$W(t) = c_1 f_1(t) + c_2 f_2(t) + \cdots\cdots + c_n f_n(t) \tag{4.8}$$

where $c_1 \cdots c_n$ are unknown coefficients which can be considered constant for a specific time interval; $f_1(t) \cdots f_n(t)$ are known base functions, e.g., unit function or ramp. Taking into account the jump variation of the coefficients in different cycles, $W(t)$ can be described by adding an input function consisting a series of unknown impulse functions As a result, unlike the traditional statistical approach where the input disturbance is described by a shaping filter, the system model is represented as

$$X_k = \Phi_{k,k-1} X_{k-1} + \delta_{k-1} \tag{4.9}$$

where δ_{k-1} is a sequence of unknown pulses appearing once every N time steps, i.e. δ_{k-1} gaines value only when $k-1 = 0, N, 2N, 3N...$ and otherwise vanishes. So an intuitive form of wave estimation can be derived using a simple deterministic model, with an assumption that the initial condition is sufficiently small ($X_0 \approx 0$), or already known. A new measurement model can be formulated from (4.2) and (4.9) for the first estimation cycle since $X_k = \Phi_{k,0} X_0 + \Phi_{k,1} \delta_0$

$$z_k^{*} = Z_k - H\Phi_{k,0} X_0 = H\Phi_{k,1} \delta_0 + V_k \tag{4.10}$$

where $1 < k \le N$. Correspondingly we can define a new state vector x_k^{*} which follows the recursive equation

$$x_k^{*} = \Phi_{k+1,k} x_{k-1}^{*} \tag{4.11}$$

where $x_0^{*} = \delta_0$ and $X_{k-1}^{*} = X_k - \Phi_{k,0} X_0 = \Phi_{k,1} \delta_0$. The measurement equation should then be written as

$$z_k^{*} = H x_{k-1}^{*} + v_k^{*} \tag{4.12}$$

Here $v_k^{*} = V_k$. The Kalman filter equations in this case will be

$$\hat{x}_{k-1}^{*} = \Phi_{k,k-1} \hat{x}_{k-2}^{*} + K_k (z_k^{*} - H\Phi_{k,k-1} \hat{x}_{k-2}^{*}) \tag{4.13}$$

$$K_k = \Phi_{k,k-1} P_{k-1} \Phi_{k,k-1}^T (H\Phi_{k,k-1} P_{k-1} \Phi_{k,k-1}^T H^T + r_k)^{-1} \tag{4.14}$$

$$P_k = (I - K_k H) \Phi_{k,k-1} P_{k-1} \Phi_{k,k-1}^T \tag{4.15}$$

where $E[V_k V_k^T] = r_k$. The driving noise term is missing here. By assuming $\hat{x}_0^{*} = 0$ and properly choosing initial covariance P_0, with equations (4.13)~(4.15), the estimates $\hat{x}_{N-1}^{*}$ can be finally achieved at the end of N time steps. Then the estimate $\hat{X}_N$ can be obtained as

$$\hat{X}_N = \Phi_{N,0} X_0 + \hat{x}_{N-1}^{*} \tag{4.16}$$

The intermediate estimates between points 0 and N can be restored as follows if necessary

$$\hat{X}_k = \Phi_{k,0} X_0 + \Phi_{N,k+1}^{-1} \hat{x}_{N-1}^{*} \tag{4.17}$$

Regarding $\hat{X}_N$ as a known initial state vector, the procedure (4.10)~(4.17) can be applied similarly for the next estimation cycle. Here the new measurement noise v_k^* includes the previous estimation error and thus is not a strictly white noise. In most cases, one can approximate v_k^* with V_k, i.e., $E[v_k^* v_k^{*T}] \approx E[V_k V_k^T] = r_k$, as usually the measurement noise is larger than the transition of previous estimation error in short period. In this way the estimates throughout the whole estimation time can be recovered. The reference is made to Salychev (1995). The characteristic feature of the above wave approach is the splitting of the total estimation time into small individual cycles consisting of N time steps. In each cycle with different pulse intensity, the Kalman filter is applied. At the end of each estimation cycle, the terminal state vector is estimated while the intermediate state vectors are achieved by restoring backward in time using the obtained terminal state vector.

4.2.2 General Procedure

By investigating the system dynamic model of INS in section 2, one can see that the initial state errors, as well as the constant sensor errors, will cause system sinusoidal oscillations at Schuler frequency. These errors are usually considered to be well calibrated through stationary alignment and kinematic calibration at point(s) where the accurate coordinate and/or gravity information are known. Eventually in the above intuitive approach, the initial errors are deliberately ignored for the consideration. However there are cases where the initial information is not exactly known and initial errors are not well calibrated. So a more general approach, which deals with not only the input disturbance but also initial errors, has to be designed for the wave estimation.

So a basic system model $X_k = \Phi_{k,k-1} X_{k-1}$ is considered, assuming the estimates of all state vector components will converge within given time period. Meanwhile introduce an additional vector e which may describe the input disturbance or approximation errors of the wave model representation. Thus, the model would be rewritten as

$$X_k = \Phi_{k,k-1} X_{k-1} + G e_{k-1} \tag{4.18}$$

$$e_k = L_{k,k-1} e_{k-1} \tag{4.19}$$

where $L_{k,k-1}$ is the transition matrix for the input disturbance vector e; G is the influence matrix. To solve the problem, the state vector can be changed:

$$X_k = X_k^0 + X_k^1 \tag{4.20}$$

where $X_k^0 = \Phi_{k,k-1} X_{k-1}^0$ with $X_0^0 = X_0$ and

$$X_k^1 = \Phi_{k,k-1} X_{k-1}^1 + G e_{k-1} \tag{4.21}$$

$$e_k = L_{k,k-1} e_{k-1} \tag{4.22}$$

where $X_0^1 = 0$. Then the estimation algorithm for one estimation cycle ($0 \le k < N$) would have the following form: (Salychev, 1995a)

For the estimation of X^0 :

$$\hat{X}_k^0 = \Phi_{k,k-1} \hat{X}_{k-1}^0 + K_k (Z_k - H\Phi_{k,k-1} \hat{X}_{k-1}^0) \tag{4.23}$$

$$\begin{aligned} K_k = {} & [\Phi_{k,k-1}P_{k-1}\Phi_{k,k-1}^T H^T - \Phi_{k,k-1}\Psi_{k-1}E[e_0 e_0^T]D_k^T H^T]\cdot[H\Phi_{k,k-1}P_{k-1}\Phi_{k,k-1}^T H^T \\ & + H_k D_k E[e_0 e_0^T]D_k^T H^T + r_k - H\Phi_{k,k-1}\Psi_{k-1}E[e_0 e_0^T]D_k^T H^T - HD_k E[e_0 e_0^T]\Psi_{k-1}\Phi_{k,k-1}^T H^T]^{-1} \end{aligned} \tag{4.24}$$

$$P_k = (I - K_k H)\Phi_{k,k-1}P_{k-1}\Phi_{k,k-1}^T + K_k HD_k E[e_0 e_0^T]\Psi_{k-1}^T \Phi_{k,k-1}^T \tag{4.25}$$

where $D_k = \Phi_{k,k-1}D_{k-1} + GL_{k-1,0}$ with $D_0 = 0$ and $\Psi_k = (I - K_k H)\Phi_{k,k-1}\Psi_{k-1} + K_k HD_k$ with $\Psi_0 = 0$.

On the basis of estimates $\hat{X}_N^0$, a new measurement equation is obtained

$$V_{k/N} = Z_k - H\Phi_{k,N} \hat{X}_N^0 = HD_k e_0 + V_k^* \tag{4.26}$$

where $V_k^* = V_k - H(\hat{X}_{k/N}^0 - X_k^0)$ with $r_k^* = E[V_k^*(V_k^*)^T]$. Thus the e-vector can be estimated using a state model $e_k = e_{k-1}$ (assuming $L_{k,k-1} = 1$).

$$\hat{e}_k = \hat{e}_{k-1} + K_k^e (V_{k/N} - HD_k \hat{e}_{k-1}) \tag{4.27}$$

$$K_k^e = P_{k-1}D_k^T [HD_k P_{k-1} D_k^T H^T + r_k^*]^{-1} \tag{4.28}$$

$$P_k = (I - K_k^e HD_k)P_{k-1} \tag{4.29}$$

With the $\hat{X}_N^0$ and $\hat{e}_N^0$ being determined, the total state vector for each epoch in the interval $t_0 \le t \le t_N$ can be restored by equation:

$$\hat{X}_k = \Phi_{k,N} \hat{X}_N^0 + D_k \hat{e}_N \tag{4.30}$$

The similar process above can be applied for the subsequent estimation cycle.

4.3 Practical Application of Filtering Procedures

4.3.1 Initial Calibration and State Observability

As mentioned in the previous section, the initial calibration of INS is critical for the system performance. Generally there are two calibration stages: one is stationary alignment at a known point; the other is kinematic calibration with supplemented measurement information.

To investigate the error behavior of an INS within initial calibration, one horizontal channel (north) is considered here under the zero-velocity and zero-Earth-rate assumption for the sake of brevity.

$$\delta \dot{v}_N = \psi_E g + \delta a_N + \delta g_N \tag{4.31}$$

$$\dot{\psi}_E = -\frac{1}{R}\delta v_N + \varepsilon_E \tag{4.32}$$

where δa_N indicates the accelerometer error in north-directed axis; ε_E is the east gyro drift; the notations for other parameters are identical to that in section 2.3. In the following discussion, the subscripts n,e will be omitted for simplicity. The objective of the calibration is to determine the initial orientation errors as well as gyro drifts and accelerometer biases. Suppose the velocity is the only available external measurement. By studying the observability of the state vector, one would find that the constant portion of accelerometer error, i.e. accelerometer bias b_a, and initial gravity disturbance are inseparable from the initial tilt error. This is much more obvious when the equation (4.31) is substituted with the integral of the equation (4.32) as shown below

$$\delta \dot{v} = g\int_0 \varepsilon dt - \omega_s^2(\delta p - \delta p_0) + g\psi_0 + \delta a + \delta g \tag{4.33}$$

where δp, position error, equals the integral of velocity error. For initial stationary alignments, the position information is usually known, and thus $\delta p_0 = 0$. The indicated velocity of INS is compared to the zero velocity reference. The observed difference is used by a built-in Kalman filter as an external measurement to align the system platform mathematically with the local level reference, and to calibrate the gyro drift. From (4.33) it is clear that the effect of three error sources, ψ_0, b_a, δg , cannot be distinguished on the basis of the stationary alignment. As a matter of fact, the acceleration error induced by the tilt error tends to cancel the sum effect of accelerometer bias and gravity disturbance during the alignment.

With provided position or velocity information from GPS, the kinematic calibration can be further performed before mission. In many cases, the initial gravity information can be somehow available for gravimetry survey. As the vehicle travels, the gravity disturbance (the vertical deflection) changes. Its difference from the initial value will decouple from the effect of tilt error. This is also the fundamentals for airborne gravimetry. As to the calibration of accelerometer bias error, it can only be achieved for strapdown INS when a maneuver motion is made by the vehicle and thus decouples the accelerometer bias from the initial tilt error. For the stabilized platform system, the decoupling between the bias and the initial tilt is impossible in this case.

Two commonly known errors not discussed thus far are the initial azimuth error and the scale factor error. Based on the gyro compass mechanization, the north orientation of computation platform can be found out or estimated to a sufficient accuracy during the stationary alignment. The remaining misalignment or nonorthogonal errors need to be further calibrated in the survey. The scale factor error of accelerometers has a feature of long-term stability. Usually it can be viewed not to change within one year once determined. Its calibration requires extensive runs in a special designed trajectory with known control points. Both the azimuth misalignment error and the scale factor error are attributed to the long wavelength error in airborne gravimetry. These two error effects could be eliminated at the end of mission if the closure information were available.

4.3.2 Choosing Initial Conditions for Kalman Filter

How well an individual calibration procedure can be achieved is mainly affected by the sensor imperfection as well as environmental fluctuation. From section 4.3.1 we have learned the fact that the initial tilt error is inseparable from the constant accelerometer bias, b_a, and the vertical deflection at the initial point, δg_0. It is quite fortunate that the sum of three error sources tends to be zero through the stationary alignment, i.e.

$$g\psi_0 + b_a + \delta g_0 = 0 \tag{4.34}$$

Then their sum effect on the system outputs can be ignored due to linearity. Since our sole purpose is to estimate the deflection difference from the initial value, the initial values for above three errors can all be set to be zero in the initialization of Kalman filter keeping in mind that the gravity disturbance should be modeled with respect to the initial point. So can their corresponding initial covariance. Sometimes the initial alignment won't be able to make the left side of equation (4.34) exactly zero due to inability to sort out the gyro drift. In this circumstance we can view this non-zero portion to be the initial tilt error and set the estimated value in its initial covariance matrix, while the initial covariance for the accelerometer bias and the vertical deflection remain zero. The constant gyro drift can not be completely calibrated in the stationary alignment. However it is reasonable to consider the gyro drift being estimated, through the alignment process, to a higher order accuracy with respect to the given value in the specification.

Some other state errors are not so critical and generally can be chosen properly at the beginning point. For instance, the initial position and velocity information are usually available with GPS measurements. The accelerometer scale factor errors are assumed to be well determined before the mission and therefore set to be zero in the simulation.

With the system model given in section 2 and initial conditions determined as above, by applying recursive Kalman filter equations (4.6) and (4.7), the change of gravity disturbance (the vertical deflection) from the initial point can be estimated. To restore the true value of gravity information along the trajectory, simply add the known initial gravity disturbance to the gravity estimates from Kalman Filter.

4.3.3 Application of Wave Estimation in Airborne Gravimetry

According to Salychev (1995), the system to which it is expedient to apply the wave method must have a bandwidth mostly in the low frequency range. Then the response to the input disturbances has the form of slowly varying oscillations. The inertial navigation system falls into this category.

Let us just investigate one horizontal channel using equations (4.31) and (4.32) for simplicity. The other channel can be analyzed similarly. Based on the intuitive concept of the wave estimation, the input disturbance should be described as a series of unknown impulses instead of a stochastic process. Thus the gravity disturbance and the gyro drift can be represented as

$$\dot{\varepsilon} = \delta^1 \tag{4.35}$$

$$\delta \dot{g} = \delta^2 \tag{4.36}$$

where δ^1, δ^2 are unknown impulses for the gyro drift and the gravity disturbance respectively. The deterministic model for this horizontal channel will be

$$\begin{pmatrix} \delta v \\ \psi \\ \varepsilon \\ \delta g \end{pmatrix}_k = \begin{pmatrix} 1 & g\Delta t & 0 & \Delta t \\ -\Delta t / R & 1 & \Delta t & 0 \\ 0 & 0 & 1 & 0 \\ 0 & 0 & 0 & 1 \end{pmatrix} \begin{pmatrix} \delta v \\ \psi \\ \varepsilon \\ \delta g \end{pmatrix}_{k-1} + \begin{pmatrix} 0 \\ 0 \\ \delta^1 \\ \delta^2 \end{pmatrix}_{k-1} \tag{4.37}$$

where Δt is the sampling interval. The Delta function on the right side can only get gain at the beginning of each estimation cycle, i.e. at $k = N, 2N, 3N, ...$ In the model (4.37) the accelerometer bias is omitted. One may consider it is added into the gravity disturbance. The omission of the accelerometer bias will not influence the determination of the difference of gravity disturbance from the initial point in this case. Suppose the initial alignment is performed fairly well, the strategy to choose initial conditions for the Kalman filter can also be applied in the wave estimation procedure. Therefore the initial conditions are set to be zero though their actual values are not. The system can be viewed as driven by unknown intensity impulses of gyro drift and gravity disturbance. The quantity to be measured is the velocity error which can be obtained by subtracting GPS measurements from INS-indicated velocities. The measurement model should then be

$$z_k = (1 \quad 0 \quad 0 \quad 0)(\delta v \quad \psi \quad \varepsilon \quad \delta g)_k^T + V_k \tag{4.38}$$

Where V_k is the measurement noise of GPS derived velocity. With the obtained system model (4.37) and measurement model (4.38), procedures (4.10)~(4.15) can be implemented to achieve the estimation of gravity disturbance.

In the intuitive form of wave estimation, we presume that the initial system errors have no effect on the gravity estimation due to their mutual cancellation. There are cases that the initial alignment is not doing well due to gyro drift and environment interruption and the non-zero sum of the left side of (4.34) has to be modeled as an initial error and needs to be estimated as well. Sometimes we also need to know how the filtering algorithm performs when some long wavelength gravity information, such as a high degree geopotential spherical harmonic model, is available. A general form for airborne gravimetry has to be formed corresponding to the approach in section 4.2.2. The gravity disturbance and the gyro drift can be considered, respectively, as comprising two parts: one is the initial constant component for each estimation cycle, which can be modeled as a bias; the other is the variation term with respect to the initial value, i.e.

$$\Delta\delta g_k = u_k + e_k^1 \tag{4.39}$$

$$\Delta\varepsilon_k = e_k^2 \tag{4.40}$$

where u_k is a roughly known value at the point of time epoch k and may be viewed as being generated by a harmonic model although it is not actually used in the following simulation ; e_k^1, e_k^2 are the input disturbance and may be viewed as a residual or approximation error of the gravity disturbance and the gyro drift respectively. Then the system model can be rewritten as

$$\begin{pmatrix} \delta v \\ \psi \\ \varepsilon \\ \delta g \end{pmatrix}_k = \begin{pmatrix} 1 & g\Delta t & 0 & \Delta t \\ -\Delta t / R & 1 & \Delta t & 0 \\ 0 & 0 & 1 & 0 \\ 0 & 0 & 0 & 1 \end{pmatrix} \begin{pmatrix} \delta v \\ \psi \\ \varepsilon \\ \delta g \end{pmatrix}_{k-1} + \begin{pmatrix} u_{k-1}\Delta t \\ 0 \\ 0 \\ 0 \end{pmatrix} + \begin{pmatrix} e_{k-1}^1\Delta t \\ e_{k-1}^2\Delta t \\ 0 \\ 0 \end{pmatrix} \tag{4.41}$$

i.e. $X_k = \Phi_{k,k-1}X_{k-1} + \bar{u}_{k-1} + Ge_{k-1}$ (4.42)

where $\bar{u}_{k-1} = \begin{pmatrix} u_{k-1}\Delta t \\ 0 \\ 0 \\ 0 \end{pmatrix}$; $G = \begin{pmatrix} \Delta t & 0 \\ 0 & \Delta t \\ 0 & 0 \\ 0 & 0 \end{pmatrix}$; $e_{k-1} = \begin{pmatrix} e_{k-1}^1 \\ e_{k-1}^2 \end{pmatrix}$; $e_k = L_{k,k-1}e_{k-1}$

Here the transition matrix $L_{k,k-1}$ can be assumed to be identity matrix.

In order to make use of the algorithm in section 4.2.2, it is required to split the state vector into two parts X_k^0 and X_k^1 as in (4.20). However the model for X_k^0 should be changed to

$$X_k^0 = \Phi_{k,k-1}X_{k-1}^0 + \bar{u}_{k-1} \tag{4.43}$$

Using (4.23)~(4.30), the initial system error as well as the input disturbance are estimated subsequently. It should be noted that, at the end of a estimation cycle, the variation components, (4.39) and (4.40), should be added into the initial gravity disturbance and gyro drift for the next estimation cycle respectively.

4.3.4 The State Convergence and the Selection of Estimation Cycle for Wave Estimation

General speaking, in the deterministic system model, the short estimation cycle has a good description of the physical process but may not be enough to allow the estimates to converge when exerting the filtering procedure. Therefore it is necessary to choose an appropriate estimation cycle time for the wave estimation by investigating the state convergence. To do so, let's first look at the estimation errors when applying a Kalman filter.

$$\hat{X}_k = \left\{ \prod_{i=1}^{k} (I - K_{k+1-i} H) \Phi_{k+1-i,k-i} \right\} \hat{X}_0 + \sum_{j=1}^{k-1} \left\{ \prod_{i=1}^{j} (I - K_{k+1-i} H) \Phi_{k+1-i,k-i} \right\} K_{k-j} V_{k-i} \tag{4.44}$$

According to Salychev (1995), the diagonal components of the first term in equation (4.44), i.e.

$$diag \left\{ \prod_{i=1}^{k} (I - K_{k+1-i} H) \Phi_{k+1-i,k-i} \right\} \tag{4.45}$$

describe the transition process of the initial estimates and meanwhile indicate the observability degree of state errors. Figure 4.1 shows the transition process of the tilt error and the gyro drift. One can easily see that it takes about 1000 sec to get convergence for the gyro drift while about 100 sec for the tilt error. This can also be verified by the gain coefficient changes of each error, as shown in Figure 4.2 and Figure 4.3.

To choose the estimation cycle for wave estimation, one has to compromise between the proper physical description of gravity disturbance and the convergence of system errors. Apparently it is impossible to choose the estimation cycle being 1000 sec so as to get complete convergence of gyro drifts. In airborne applications, one consideration is to set the estimation cycle around 100 sec, equivalent to the convergent time of tilt error. We will see the different results with regard to different estimation cycle in the following.

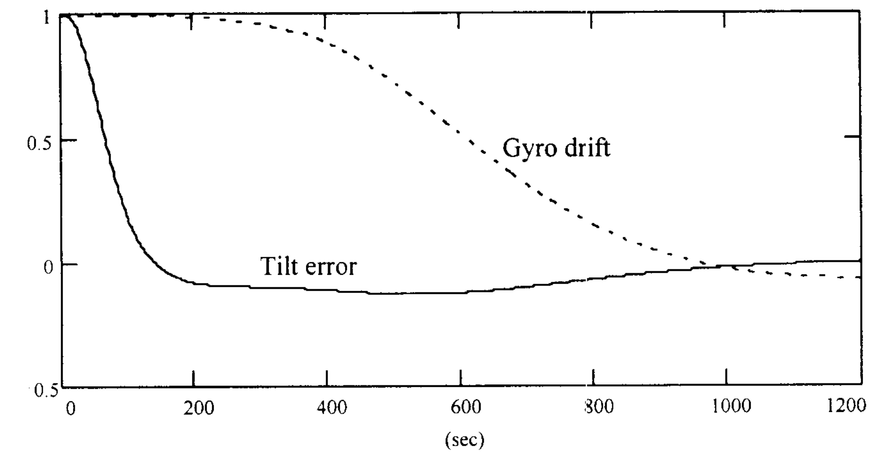

Fig. 4.1 The transition process of initial estimates for the tilt error and the gyro drift

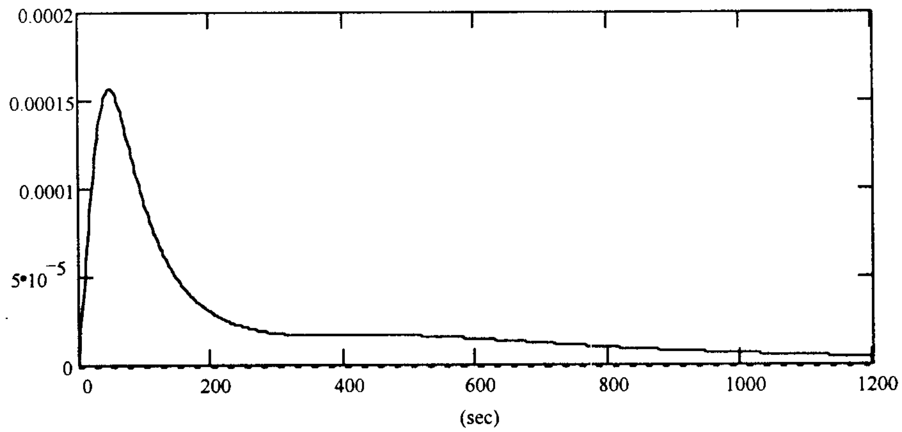

Fig. 4.2 The gain coefficients changes for tilt error

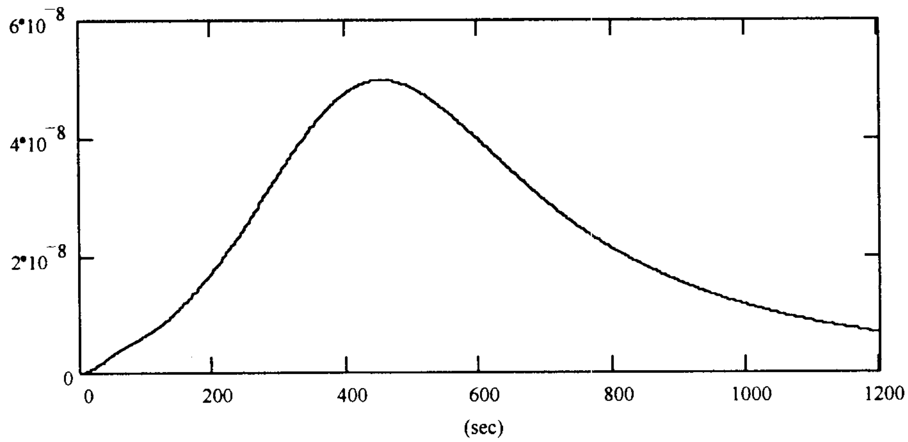

Fig. 4.3 The gain coefficients changes for gyro drift

5 SYSTEM SIMULATIONS

In principle, all the physical systems can be simulated mathematically according to their dynamics. From a theoretical point of view, system simulations are by all means an economic and flexible way to investigate system behaviors under various circumstances, to verify a proposed new approach to some extent and to provide some necessary orientations for the real test. Based on the parameters specified by manufacturer in the system manual, under a certain assumption, the dynamic characteristics of LN-93 inertial system, as well as GPS, are simulated for this study. Then the proposed methods, Kalman filtering and wave estimation, are applied using the generated data from the simulation.

5.1 The Generator of Gaussian Pseudorandom Numbers

In a linear stochastic system, the Gauss white noise process is considered as an important driving input, which determines the statistical characteristics of the system. In principle, the white noise is a stationary and uncorrelated process. The ideal white noise process is physically unreachable due to its infinite variance nature. However, under reasonable assumptions of the physical nature of the process, we can make use of white noise concepts approximately. For example, we may assume the process has no correlation up to frequencies defined by the small sampling interval. For the smaller intervals the process may indeed be correlated and the PSD drops to zero. Then the variance is also finite. In order to achieve this white noise process computationally, the discrete white noise process at a specific time t_k can be viewed as the continuous average of the continuous white noise process over a small interval Δt, i.e.

$$W_k = \frac{1}{\Delta t}\int_{t_k-\Delta t}^{t_k} W(t) \tag{5.1}$$

where W_k, $W(t)$ represent discrete and continuous white noise respectively. The following equalities exist:

$$E[W_k] = E[W(t)] \tag{5.2}$$

$$\begin{aligned} E[W_k^{\,2}] &= \frac{1}{(\Delta t)^2}\int_{t_k-Dt}^{t_k}\int_{t_k-Dt}^{t_k} E[W(t)W(t)dtdt \\ &= \frac{1}{(\Delta t)^2}\int_{t_k-Dt}^{t_k}\int_{t_k-Dt}^{t_k} q\delta(t-\tau)dtdt \\ &= q / \Delta t \end{aligned} \tag{5.3}$$

Assuming the distribution of random variables of the white noise process are the Gaussian distribution with zero mean, a standard algorithm can be used to generate the above Gaussian white noise process. Actually, it is a pseudorandom process as it is not absolutely "white" (Gao, 1989).

First of all, uniformly pseudorandom numbers need to be generated for the use of Gaussian pseudorandom numbers' generation, according to the following recursive equation:

$$Ux_k = 259.0 \times Ux_{k-1} - \text{int}(259.0 \times Ux_{k-1}) \tag{5.4}$$

where Ux_k are supposed to be the generated uniformly pseudorandom numbers between 0 and 1, and its initial value can be simply obtained from equation: $Ux_0 = Ix / 32767$ (Ix is an odd integer initially given between 0 and 32767. Different Ix value yields different pseudorandom process). The int( ) in equation (5.4) is an integer function. With the uniformly pseudorandom numbers obtained, then, the Gaussian pseudorandom process can be realized consequently as follows

$$Gx_i = (\sum_{j=1}^{12} Ux_{i\times12+j} - 6.0) \times SD + M \tag{5.5}$$

where Gx_i are the generated Gaussian pseudorandom sequence, from above algorithm, with a standard deviation SD and a mean value M

.

5.2 Numerical Integration

In a physical system, like INS, the system dynamics as well as the error behavior are often described by a set of first-order linear differential equations, e.g., equations (2.2) and (2.10). To solve these equations for the purpose of simulation, numerical integration has to be performed.

Generally, the differential equation can be expressed as

$$\dot{y} = f(t, y) \tag{5.6}$$

where y is either a scalar quantity or a vector, with initial value $y(t_0) = y_0$; The function $f(t, y)$ should be reasonably smooth in order to guarantee the existence of solution for the differential equation. Therefore the solution of equation (5.6) can be represented by Taylor's series:

$$y(t) = y(t_0) + \Delta t\, \dot{y}(t_0) + \frac{(\Delta t)^2}{2!} \ddot{y}(t_0) + \frac{(\Delta t)^3}{3!} \dddot{y}(t_0) + \cdots\cdots \tag{5.7}$$

As to the small interval $\Delta t = t - t_0$, we can truncate the higher order of Taylor's series and obtain an approximated solution of differential equation (5.6), e.g., considering only up to the first-order derivative term.

$$y(t) \approx y(t_0) + \Delta t\, \dot{y}(t_0) \tag{5.8}$$

This is the so-called Euler equation for the numerical integration. It is noted that as higher order terms are added to equation (5.8), the more accurate the numerical integration becomes. However, the higher order derivatives are sometimes complicated or even not achievable. So in practice the higher-order Taylor methods are seldom directly applied but indirectly used in the following Runge-Kutta method, which is more efficient and accurate.

Based on the differential theorem

$$\frac{y(t) - y(t_0)}{\Delta t} = \dot{y}(t_0 + \vartheta \Delta t) \tag{5.9}$$

where $0 < \vartheta < 1$. A set of fourth-order Runge-Kutta equations is given as

$$y(t) = y(t_0) + \frac{\Delta t}{6}(K_1 + 2K_2 + 2K_3 + K_4) \tag{5.10}$$

$$K_1 = f(t_0, y(t_0)) \tag{5.11}$$

$$K_2 = f(t_0 + \frac{\Delta t}{2}, y(t_0) + \frac{\Delta t}{2} K_1) \tag{5.12}$$

$$K_3 = f(t_0 + \frac{\Delta t}{2}, y(t_0) + \frac{\Delta t}{2} K_2) \tag{5.13}$$

$$K_4 = f(t_0 + \Delta t,\ y(t_0) + \Delta t K_3) \tag{5.14}$$

5.3 Simulated System Errors and Gravity Disturbance

System dynamic characteristics are very much related to the vehicle kinematic condition. In the simulation, it is assumed that the airplane flies at a constant speed of 360 km/hr, with a fixed height and without changing directions. The smooth gravity signature is first considered. According to the system mechanization and error models given in section 2, the LN-93 inertial system is simulated using the specified parameters.

In the following figures (Fig. 5.1--Fig. 5.4), some of the simulated system error features are presented. They are accelerometer errors ($acc\_err_{t,i}$), gyro drifts ($gyro\_drf_{t,i}$), platform attitude errors ($att\_err_{t,i}$) with respect to local level n-frame and earth-referenced vehicle velocity errors ($vel\_err_{t,i}$). Here the subscript "t" in each parameter means time and the subscript "i", with value of 1,2 and 3, indicates north, east and down directions respectively. The accelerometer and gyro errors indicate a constant bias with certain amplitude of noise characteristics. Attitude errors and velocity errors should reveal a mixed oscillation of Earth's spin rate and Schuler frequency which is modulated by the Foucault frequency. However from the figures these features are not apparently seen due to the short time scale.

The present interest is in understanding the estimation of the gravity disturbance, so the GPS is simply viewed as providing direct observations of position. Therefore the error is modeled as a bias with white noise. Actually, for the estimation of acceleration, the GPS position bias has no effect. The following GPS-derived accelerations (Fig. 5.5) are obtained by smoothing over a period of 60 seconds. In Fig.5.5, the subscripts "t" and "i" of the legend ($gps\_acc_{t,i}$) have the same meaning as in Fig. 5.1~5.4. Here only horizontal effects are considered (i=1,2).

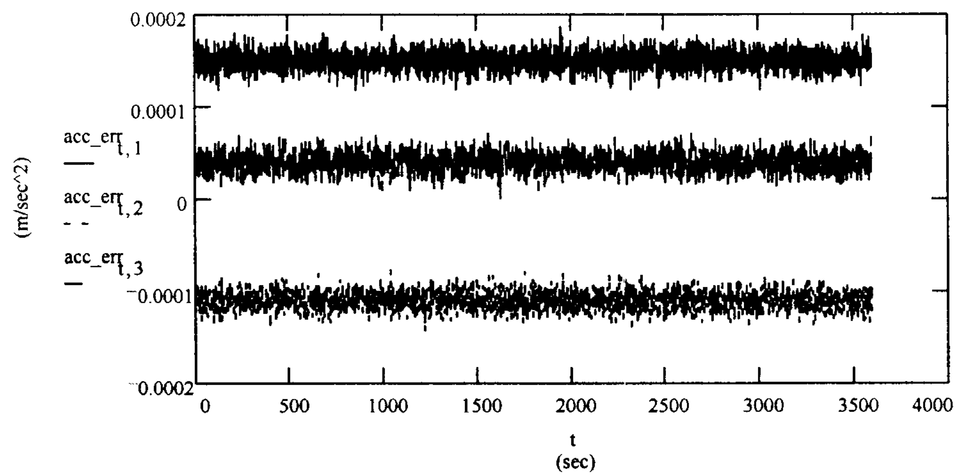

Fig 5.1 Simulated accelerometer errors

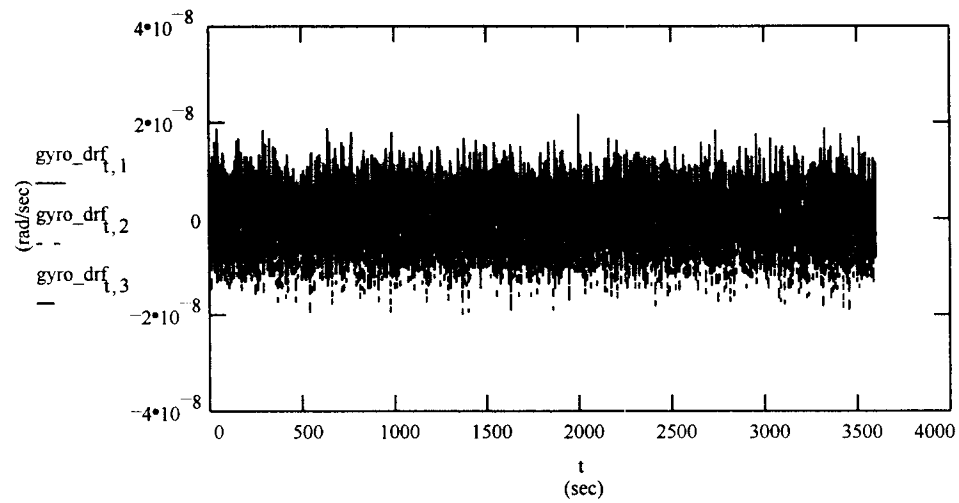

Fig 5.2 Simulated gyro drifts

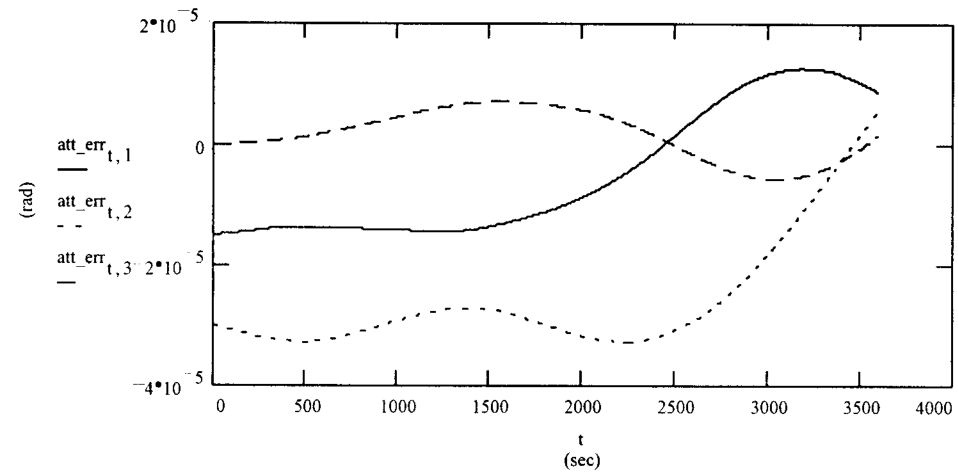

Fig 5.3 Derived attitude errors

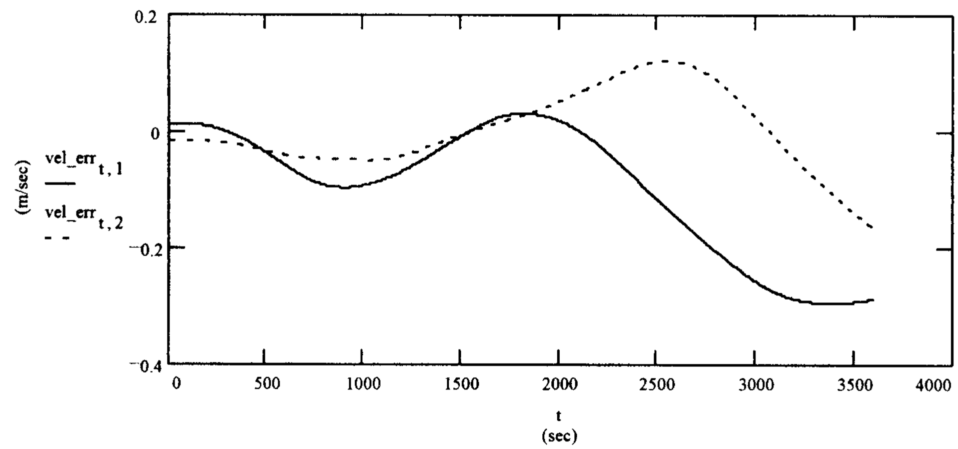

Fig 5.4. Derived horizontal velocity errors

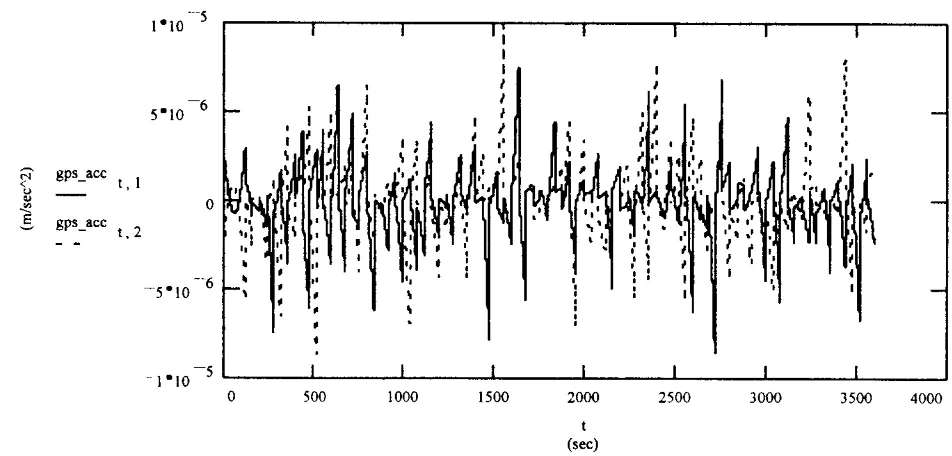

Fig 5.5 GPS-derived acceleration errors

Fig 5.6. shows the simulated gravity disturbances ($dg_{t,i}$) in the horizontal channels (i=1,2) for baseline gravity signature, using the third-order Gauss-Markov models.

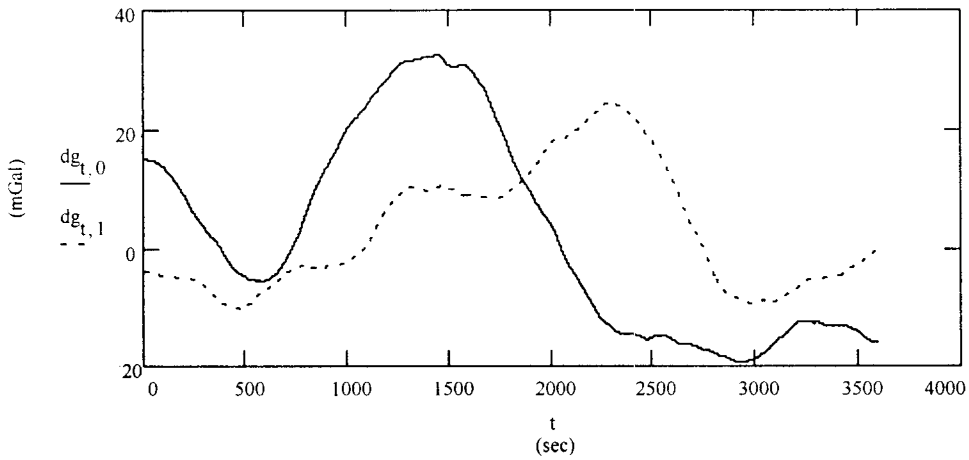

Fig 5.6. Simulated along-track gravity disturbances in horizontal direction (baseline)

6. Filtering Results and Discussions

With the simulated data, estimation approaches, like the Kalman filter and wave estimation, can be finally implemented to estimate the gravity vector. In the Kalman filter, the position updates of GPS are taken as direct observations, while in the wave estimation, the observations, being velocities, need to be constructed by differencing each two neighboring positions in time.

6.1 Straight Line Survey under Different Circumstances

In this simulation, the survey trajectory is first designed to be a straight line. The airplane is supposed to be flying at a constant speed of 360 km/hr, with an azimuth of 45 degree. The baseline gravity field is adopted.

6.1.1 Implementing of Kalman Filter and Wave Estimations

First of all, let's consider the occasion that the initial alignment is ideally fulfilled, i.e. $g\psi_{E0}+b_{a_N}+\delta g_{N0}=0$ and $-g\psi_{N0}+b_{a_E}+\delta g_{E0}=0$, and the constant gyro drift is fully estimated (for east gyro, we have $\psi_{D0}\omega_e\cos\varphi+b_{\varepsilon_E}=0$). Under this assumption, the initial estimates as well as the initial covariance can be set to zero since the effects of these initial errors cancel each other when it comes to the estimation of gravity vector difference with respect to the initial point. With the proposed filtering approaches in section 4, the estimation process can be performed.

Figures 6.1~6.3 show the estimated results with Kalman filter, intuitive method (which can only deal with input disturbances) and general wave estimation (which estimates initial states as well as input disturbances) respectively. For the present situation, both wave estimations seek to resolve the gravity disturbance regardless of initial conditions. The estimation cycle for wave estimation here is 80 sec. The corresponding root mean square errors (RMS) are given in the right side block. The solid line in the Figures indicates the estimation error in north direction while the dotted line in east direction unless otherwise illustrated in the following.

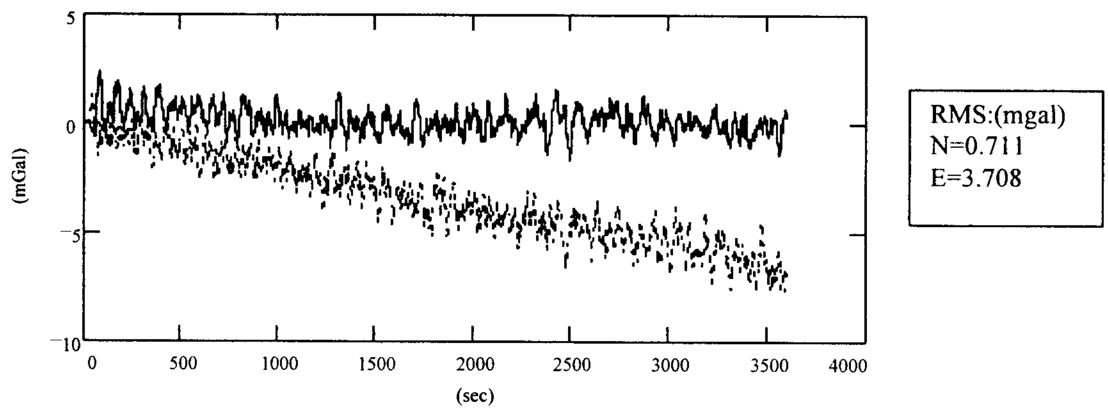

Fig. 6.1 The estimation errors for gravity vector disturbance by Kalman filter (ideal alignment)

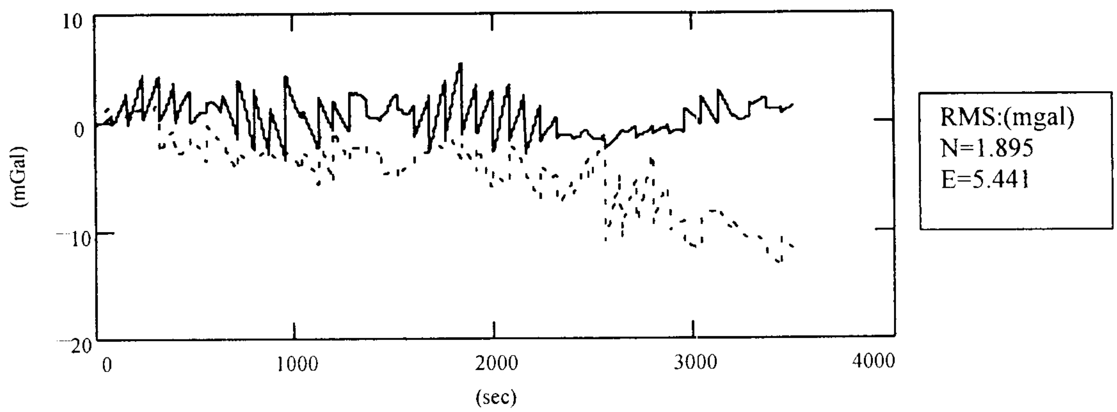

Fig 6.2 The estimation errors for gravity vector disturbance by intuitive wave estimation (ideal alignment; T=80 sec)

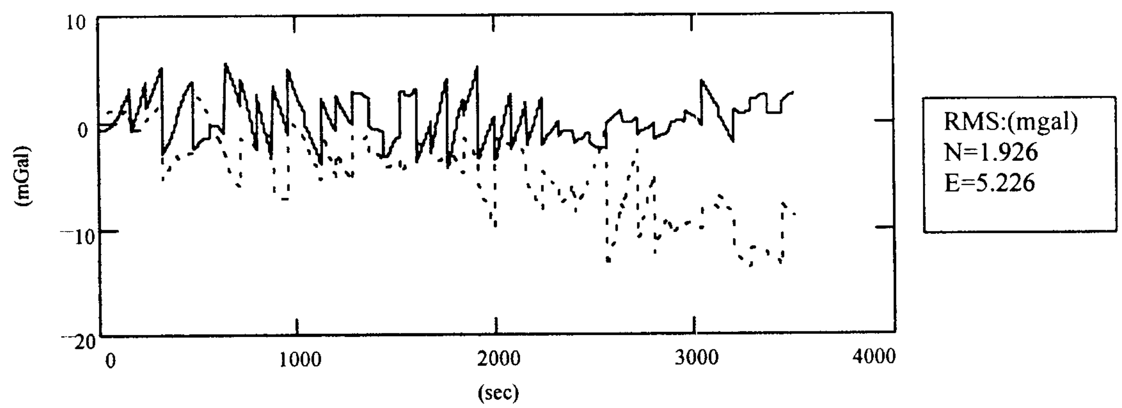

Fig 6.3 The estimation errors for gravity vector disturbance by general wave estimation (ideal alignment; T=80 sec)

From the figures, one can see that, in addition to long wavelength error tendency, the estimation errors by Kalman filter contain small high frequency components while the estimation errors by wave estimation reveal discontinuities at the end of each estimation cycle. Both high frequency features and discontinuities can be smoothed if a polynomial function is fit to the obtained estimates, as will be shown later. In terms of maximum errors in one hour, the Kalman filter performs better than the wave estimation. This can be explained since the Kalman filter has an advantage of accounting for long wavelength errors, like the azimuth error, while the wave estimation does not. The root mean square errors with respect to the three cases (Fig 6.1~6.3) are subsequently 0.711 mgal, 1.895 mgal, 1.926 mgal for the north direction component, and 3.708 mgal, 5.441 mgal, 5.226 mgal for the east direction component. The intuitive approach and general wave estimation do not show much accuracy difference in terms of root mean square errors. Since the intuitive wave estimation has an inability to deal with the initial state errors assuming they are sufficiently small or already known, we will not consider this approach in the underlying discussions.

As discussed in the previous section, the initial stationary alignment tends to make platform errors cancel the sum of initial gravity disturbance and the accelerometer bias. But in most cases, this process can never be done, i.e. $g\psi_{E0} + b_{a_N} + \delta g_{N0} \neq 0$ and $-g\psi_{N0} + b_{a_E} + \delta g_{E0} \neq 0$, due to environmental interruptions etc. The same holds for the gyro compass process, i.e. $\psi_{D0}\omega_e \cos\varphi + b_{\varepsilon_E} \neq 0$. It is reasonable to attribute the sum of each of above three equations to just one of the relevant errors. For instance, the residual of ($g\psi_{E0} + b_{a_N} + \delta g_{N0}$) can be considered as induced only by the initial platform error while the accelerometer bias error as well as initial gravity disturbance can be assumed zero. The residual of ($\psi_{D0}\omega_e \cos\varphi + b_{\varepsilon_E}$) at alignment can be viewed solely as a gyro drift while the initial azimuth error can similarly assumed zero. Based on this strategy, the presumed initial tilt errors, indicating the residual of the corresponding channel, are supposed here to be one order smaller than their actual values after the initial alignment. In other words, the actual initial tilt error is a few arcsec but the presumed residual error reduces to about several tenth of arcsec. Similarly the presumed constant gyro drift residual turns out to be 0.0003 deg/hr while the actual gyro drift is still 0.003 deg/hr. To make the discussion simple and clear, we will refer the case without residual errors as ideal alignments, the case which reduces the presumed initial tilt errors and gyro drifts one order smaller as good alignments and the case with half order smaller initial errors as tolerable alignments.

Figures 6.4~6.7 show the filtering results in good alignments case. Only Kalman filter and general wave estimation procedures are applied here. Three estimation cycles, T=50, 80 and 120 sec, are chosen for the wave estimation for comparison.

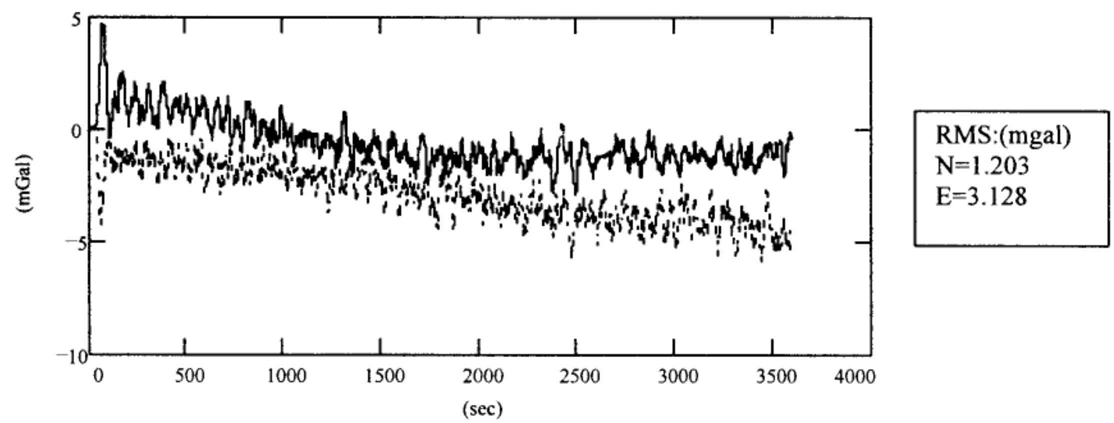

Fig. 6.4 The estimation errors for gravity vector disturbance by Kalman filter (good alignment)

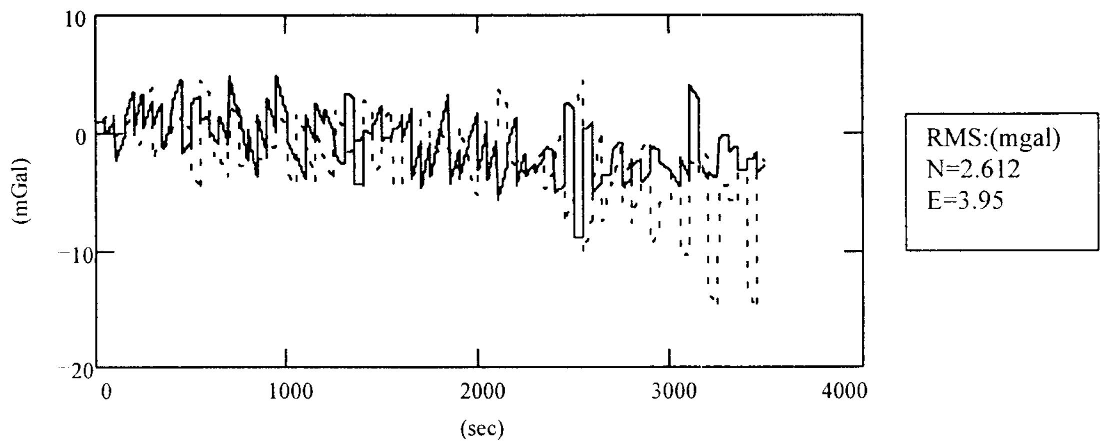

Fig. 6.5 The estimation errors for gravity vector disturbance by wave estimation (good alignment; T=50 sec)

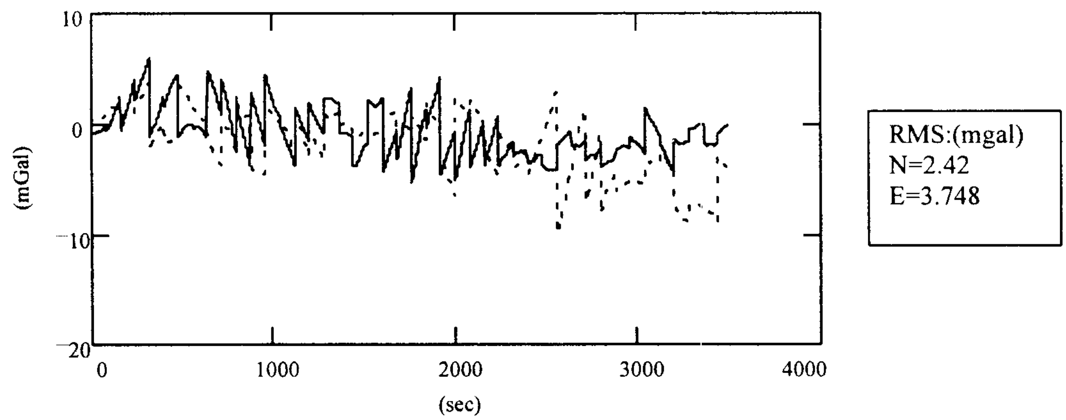

Fig. 6.6 The estimation errors for gravity vector disturbance by wave estimation (good alignment; T=80 sec)

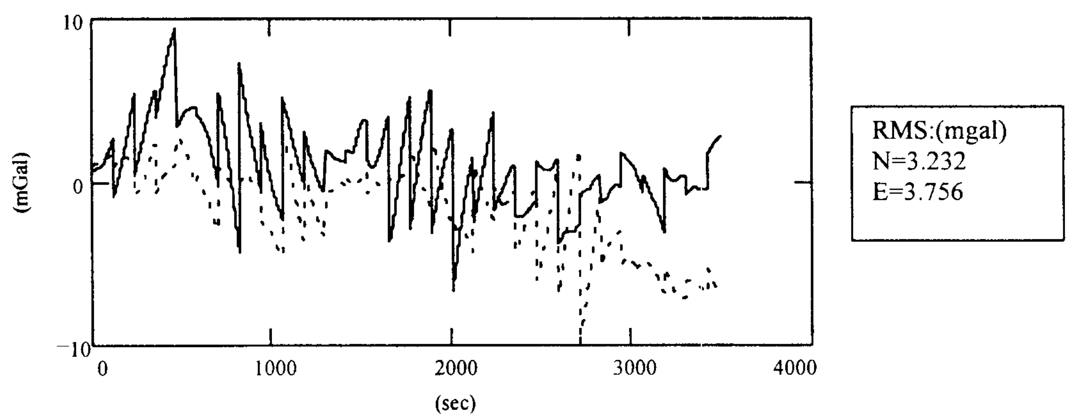

Fig. 6.7 The estimation errors for gravity vector disturbance by wave estimation (good alignment; T=120 sec)

By comparing the RMS errors, one may find the filtering result of north direction in ideal alignments (Figures 6.1~6.3) is better than that in good alignments (Figures

6.4~6.7) with both filtering methods. However, unexpectedly, it is the other way around in the east components. The reason for this needs to be further investigated. But generally the larger the residual initial errors are, which means less success in the initial alignment, the worse the achieved filtering results would be, as will be shown later. It can also be noted that the most appropriate estimation cycle for wave estimation should be 80 sec with airplane speed of 360 km/hr. This estimation cycle might vary depending on the vehicle speed. We will see this in the next section.

Figures 6.8~6.9 show the results of the tolerable alignment occasion. Obviously the estimation errors indicated in the Figures 6.8 and 6.9 are not as good as those in Figures 6.4 and 6.6. From this it has been verified that the performance at initial alignment directly affects the achievable gravimetry results in a way stated in the last paragraph.

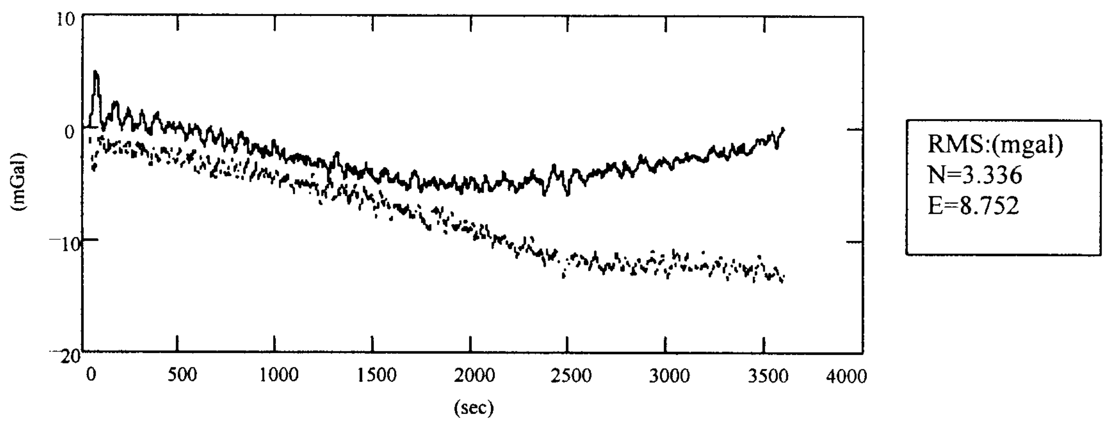

Fig. 6.8 The estimation errors for gravity vector disturbance by Kalman filter (tolerable alignment)

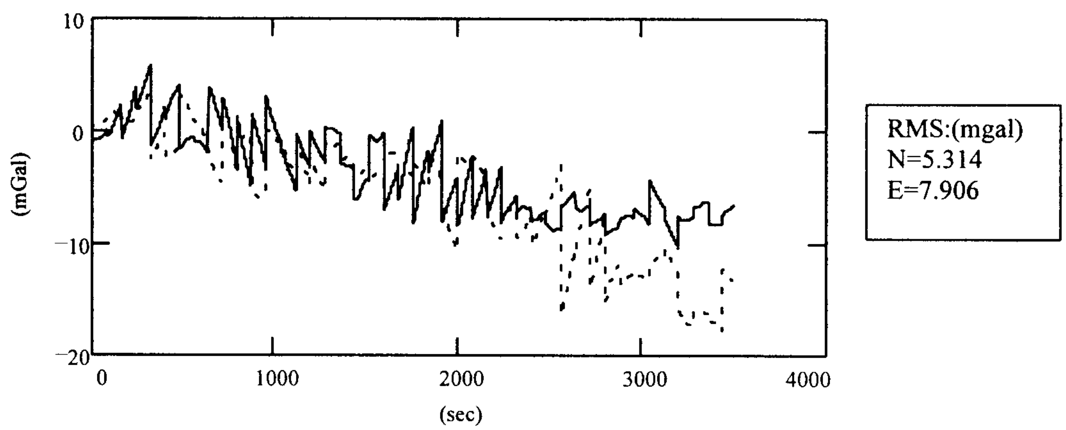

Fig. 6.9 The estimation errors for gravity vector disturbance by wave estimation (tolerable alignment; T=80 sec)

6.1.2 The Effect of Vehicle Speed on the Determination of Estimation Cycle

To choose the appropriate estimation cycle for wave estimation, one has to consider the influence of vehicle speed. Generally the convergence of state errors is associated with the time only but the gravity modeling depends on the distance traveled with respect to that time. As mentioned at the beginning of this chapter, the long estimation cycle is good for the state convergence but is not adequate for representing the gravity field using a deterministic model. It is anticipated that, with the lower vehicle speed, the appropriate estimation cycle for wave estimation could be set longer.

To investigate the proposed issue, the vehicle speed in the simulation is deliberately set to be 180 km/hr, equal to half of the airborne speed in the previous discussion. So, within one hour, the vehicle only travels half way of the gravity field shown in Fig. 5.6. Since our purpose here is to check the estimation cycle, only wave estimation results are given with three different cycles as shown in Fig. 6.10~6.12. Comparing the three figures, one

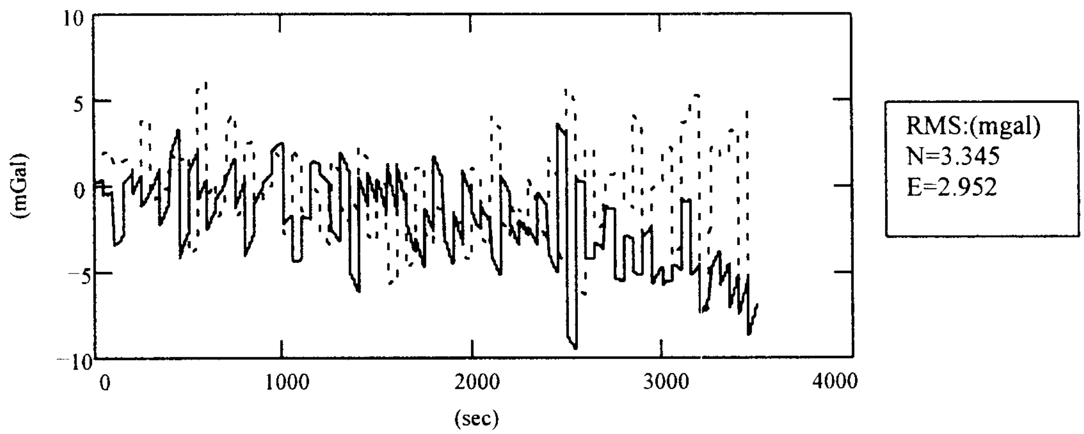

Fig. 6.10 The estimation errors for gravity vector disturbance by wave estimation (v=180 km/hr, T=50 sec)

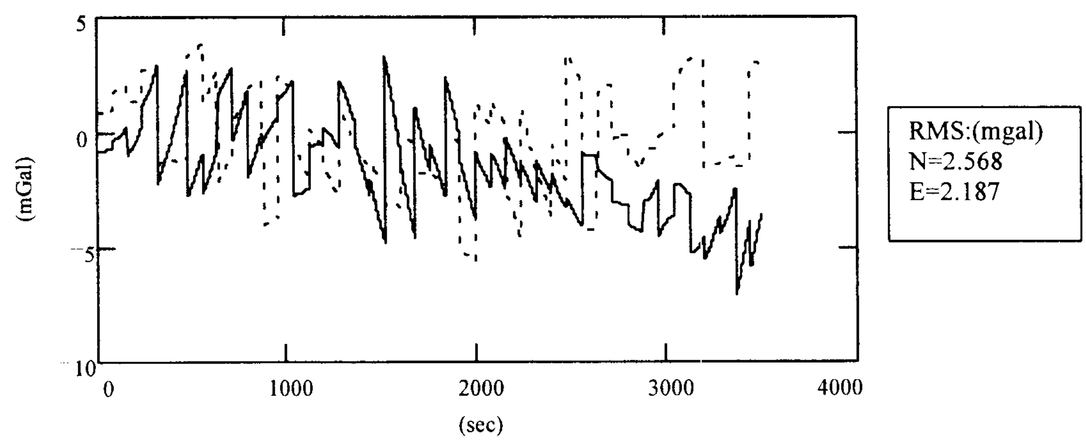

Fig. 6.11 The estimation errors for gravity vector disturbance by wave estimation (v=180 km/hr, T=80 sec)

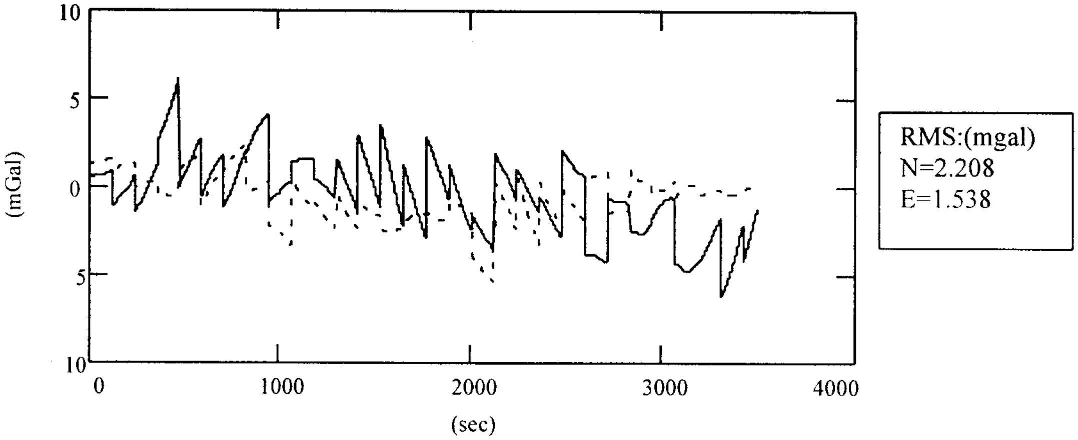

Fig. 6.12 The estimation errors for gravity vector disturbance by wave estimation (v=180km/hr, T=120 sec)

can see that the result in Fig. 6.12 appears to be better than the others in Fig. 6.10 and 6.11 in terms of estimating accuracy (RMS), which means the appropriate estimation cycle in this case should be 120 sec.

Since our interests here are airborne gravimetry, we will stick to 360 km/hr airplane speed and 80 sec estimation cycle for the wave estimation. Also the occasion with good alignments is considered the usual case for the following discussions.

6.1.3 The Effect of Different Gravity Field

Through the spectral study, it was shown that the gravity disturbance, being a desired useful signal, acts as a major error source as well. The effect of rough gravity signature (Fig. 6.13) on the estimation performance in the filtering procedure is illustrated in Figures 6.14 and 6.15. It can be roughly seen that the estimation errors by both Kalman filter and wave estimation are oscillating intensively and the long wavelength error terms are more significant as compared to those with baseline signature (Fig. 6.4 and Fig. 6.6)

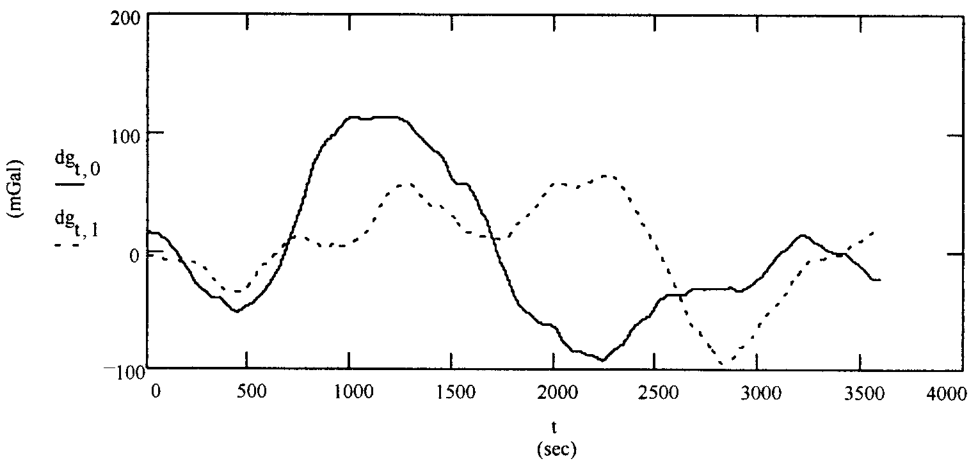

Fig. 6.13 Simulated along-track gravity disturbances in horizontal direction (rough)

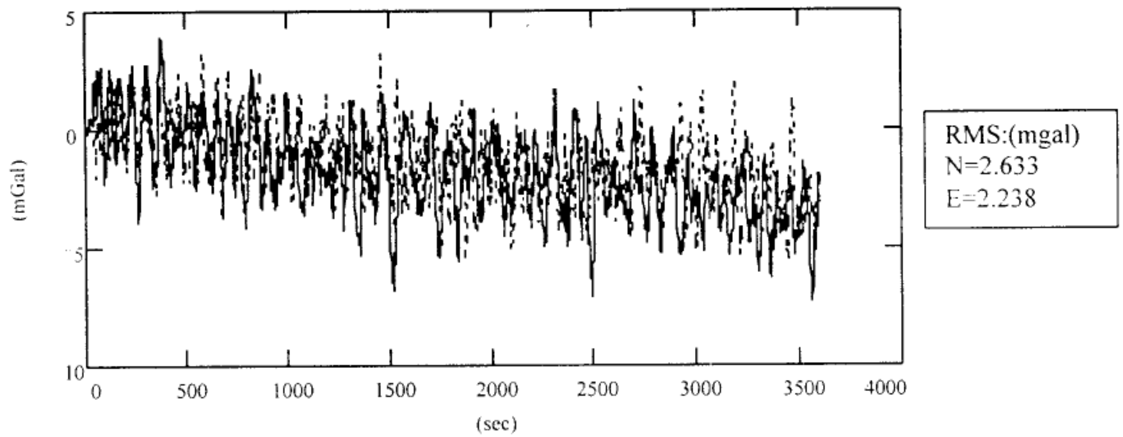

Fig. 6.14 The estimation errors for gravity vector disturbance by Kalman filter (rough gravity field)

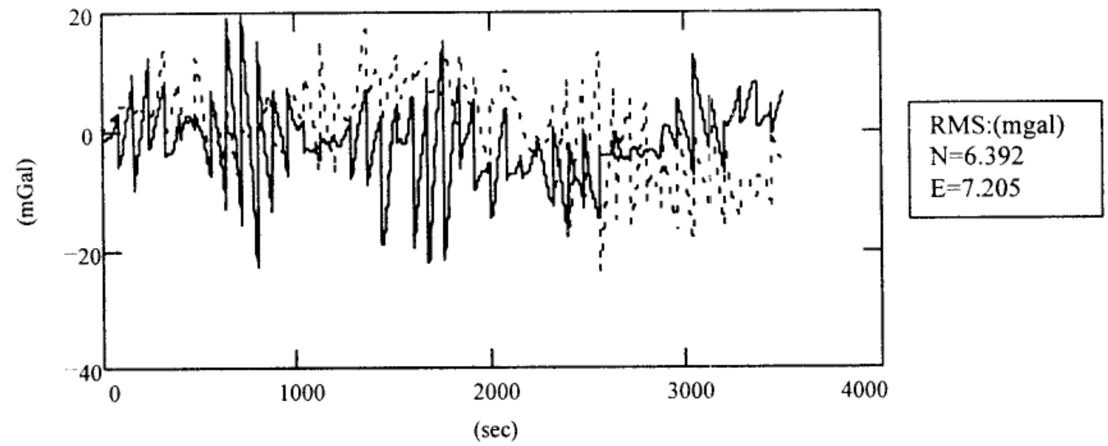

Fig. 6.15 The estimation errors for gravity vector disturbance by wave estimation (rough gravity field; T=80 sec)

In all the above discussions, the gravity disturbance model is limited to the Gauss Markov process. Occasionally in some special regions, the gravity may change sharply, in which case the Gauss Markov model may not apply. To investigate the influence of this model error on the performance of the Kalman filter and the wave estimation, a trapezoid gravity field change within half an hour is presumed as denoted in Fig. 6.16. The filtering results are given in Fig. 6.17 and Fig. 6.18. At the sharp changing point of the gravity field, one can see the estimation errors tend to be unstable for either filtering approach. It seems that the Kalman filter performs better than the wave estimation in this situation.

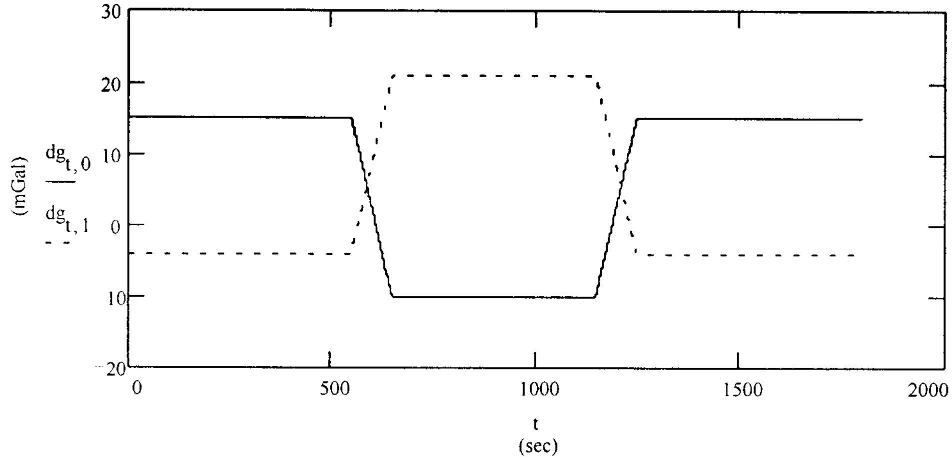

Fig. 6.16 Simulated along-track gravity disturbances in horizontal direction (trapezoid)

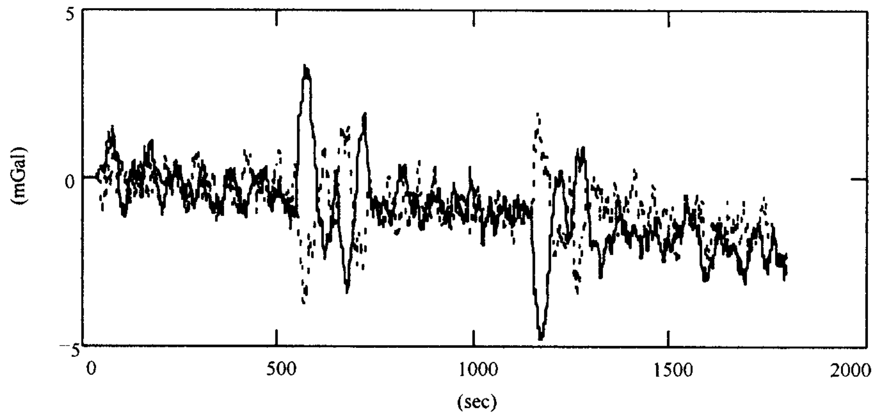

Fig. 6.17 The estimation errors for gravity vector disturbance by Kalman filter (trapezoid gravity field)

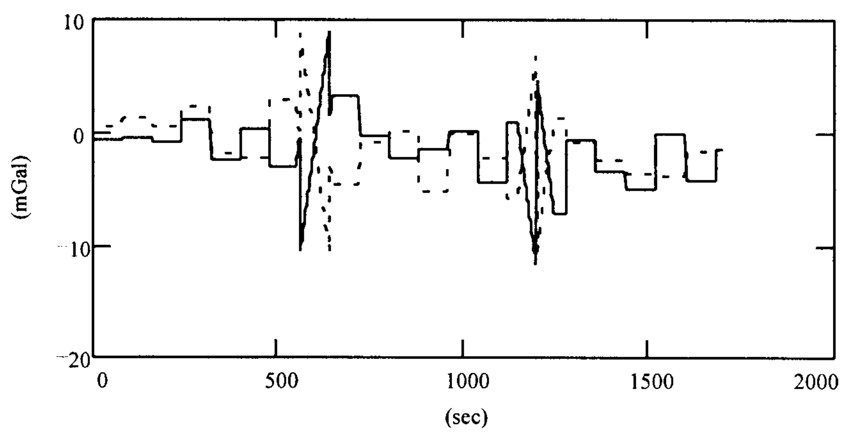

Fig. 6.18 The estimation errors for gravity vector disturbance by wave estimation (trapezoid gravity field; T=80)

6.2 The Effects of a Change in Trajectory on Estimation Accuracy

A change in trajectory will affect the system dynamics to some extent according to the system error model in section 2.3. In the practical application of filtering procedures, some system error residuals, like the azimuth error and gyro drifts, may cause different gravimetry errors depending on the travel routine. It is necessary to understand the effects of a specific trajectory on gravity disturbance recovery. Two typical trajectories are presented here. The simulation is base on the good alignment. The estimation cycle for wave estimation is 80 sec.

6.2.1 L-shape Trajectory

The above discussions are based on the straight-going mission without changing directions. In the case of vehicle direction changes, with the baseline gravity field, it is assumed here that the airplane first flies towards north at a constant speed of 360 km/hr for about half an hour, and then makes a right circular turn with a radius of one kilometer towards the east, and then keeps flying towards east for the rest of the hour. The obtained filtering results are shown in Fig. 6.19~6.20.

From the figures, it can be noted that there is a trend change of estimation errors between the first half hour and the second half hour as compared to the same situation in a straight line trajectory (Fig. 6.4 and Fig. 6.6), which may indicate some system errors, e.g. the azimuth error, have different effects in the two legs of the L-shape trajectory.

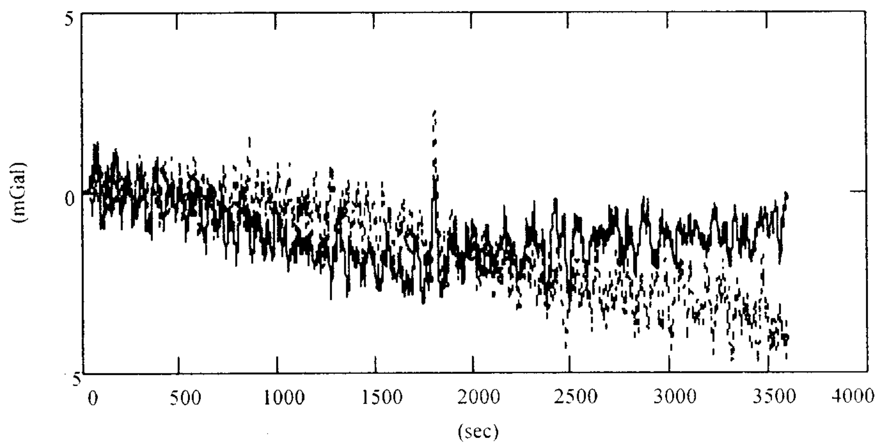

Fig. 6.19 The estimation errors for gravity vector disturbance by Kalman filter (L-shape)

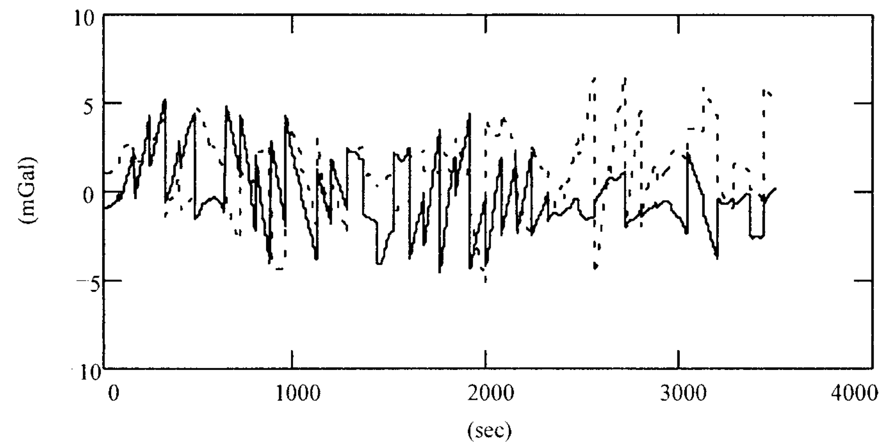

Fig. 6.20 The estimation errors for gravity vector disturbance by wave estimation (L-shape)

6.2.2 Circular Trajectory

It has been known that information in the form of closure in gravity should help improve gravity recovery. Here we deliberately assume the airplane is flying along a circular trajectory, e.g. a closed circle with a radius of about 60 km. The magnitude of the velocity vector is kept at 360 km/hr. As the airplane flies back to the beginning point, the closure gravity information can be obtained and thus used to smooth or adjust the intermediate estimating results. It is supposed in the simulation that the gravity signature between the first half circle and the second one is symmetrical, so that the actual gravity disturbance at the end of mission is the same as that of the beginning point.

Fig. 6.21 and Fig. 6.22 show the estimation errors by filtering procedures. The curve-fitting process is applied to obtain the gravity estimates as will be shown in the next section. And the RMS errors, with and without closure information, will be given for comparison.

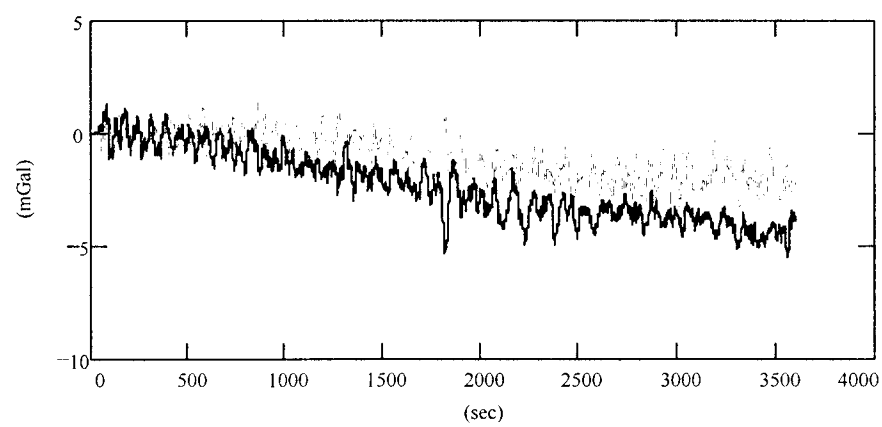

Fig. 6.21 The estimation errors for gravity vector disturbance by Kalman filter (circle)

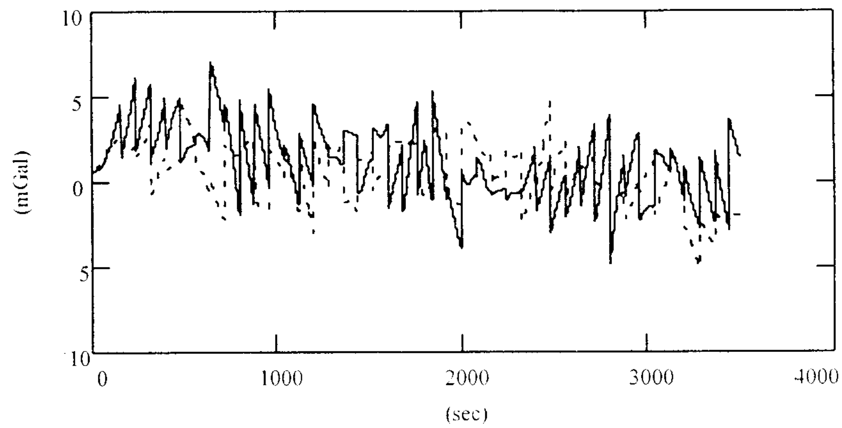

Fig. 6.22 The estimation errors for gravity vector disturbance by wave estimation (circle)

6.3 Smoothing Estimates Using Polynomial Function Fitting

The estimation errors above retain some high frequency spikes or reveal a large oscillation. This portion of errors can be largely smoothed when fitting estimates with a polynomial function, e.g. a 5th-order polynomial, and applying interpolation. Fig. 6.23~6.26 show the smoothing results after polynomial fitting for the occasion of straight going mission with good alignments. The solid line here indicates the true gravity disturbance while the dotted line denotes the estimates. It has been shown that the estimates, after smoothing, reproduce the true gravity disturbance to a fair extent. Similarly the estimates for the other occasions can also be performed. The summary results in terms of root mean square errors (RMS) are given in next section.

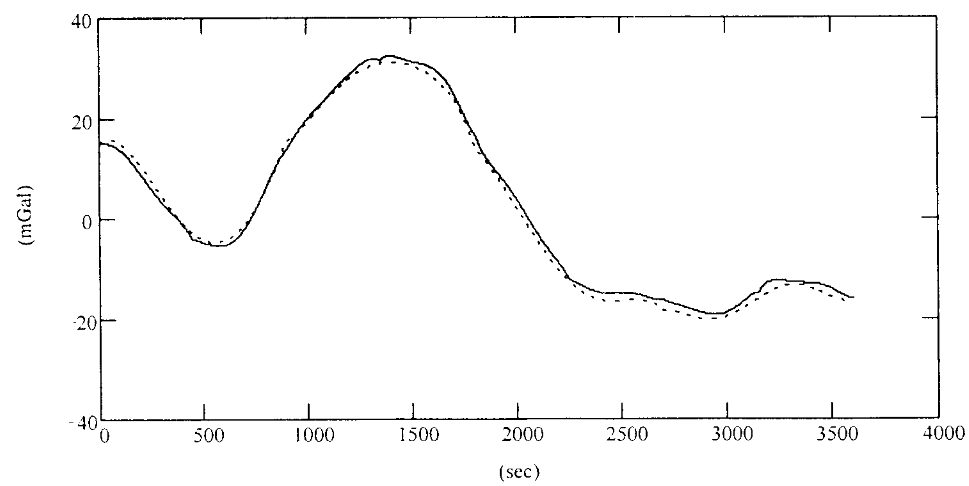

Fig. 6.23 The estimated north gravity disturbance versus its true value by Kalman filter and after a 5th order polynomial fitting process

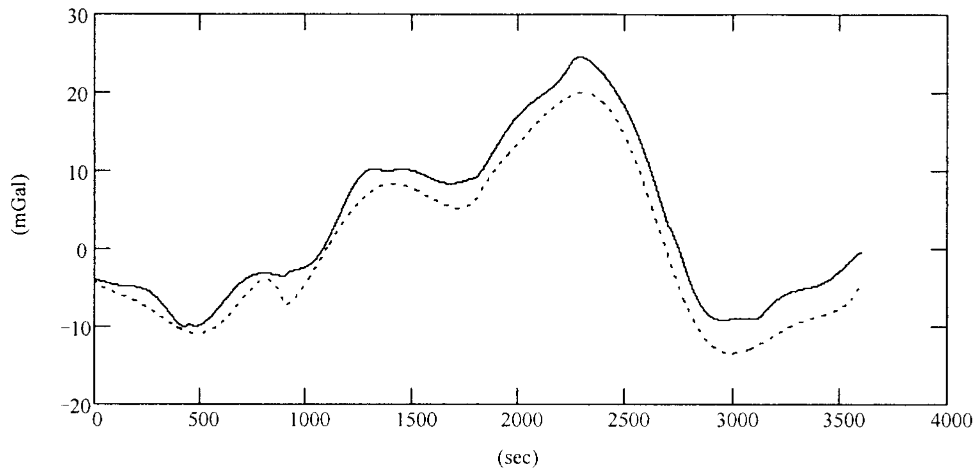

Fig. 6.24 The estimated east gravity disturbance versus its true value by Kalman filter and after a 5th order polynomial fitting process

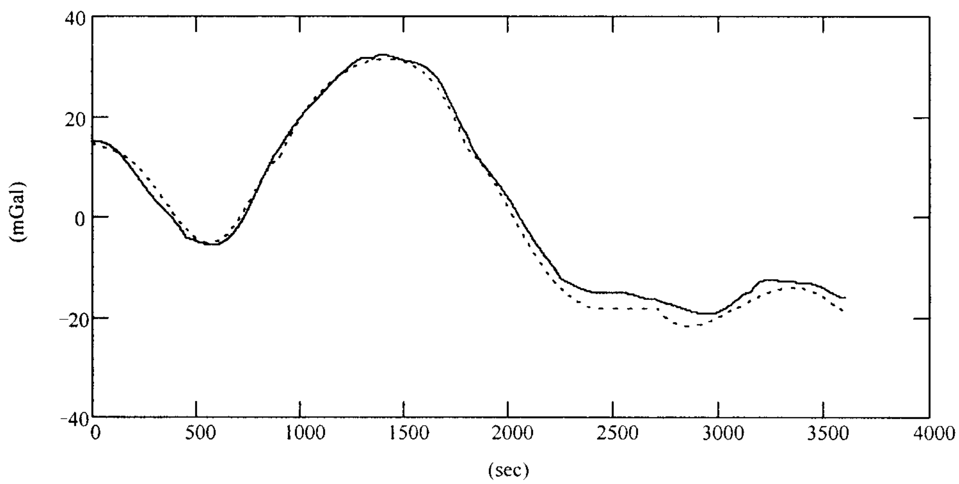

Fig. 6.25 The estimated north gravity disturbance versus its true value by wave estimation and after a 5th order polynomial fitting process

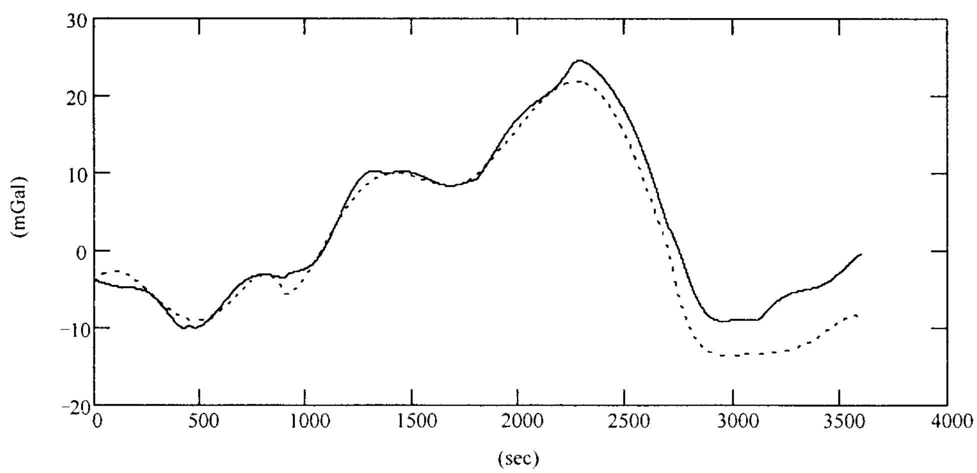

Fig. 6.26 The estimated east gravity disturbance versus its true value by wave estimation and after a 5th order polynomial fitting process

7. CONCLUSION

To study the feasibility of the gravity recovery, especially the vertical deflection, of the airborne strapdown inertial system combined with differential GPS, a spectral analysis has been performed according to the error contributions of the two systems to airborne gravimetry. Both systems are also simulated, with the specified system parameters for LN-93 and with up-to-date achievable accuracy values for DGPS. Finally the most common used estimation approaches, Kalman filter and wave estimation, are applied using the simulated data. A summary of estimation errors for different trajectories are given in the Table 7.1 without closure gravity information at the end of mission, and Table 7.2 with closure gravity information and a linear adjustment being applied. For circle case, the traverse is a closed loop and the gravity disturbance at the end point equals to that at the beginning point. All results here are achieved under the circumstance of good alignments as defined in the section 6.2. In the straight-line occasion, the results from three cases: velocity v=360 km/hr and v=180 km/hr, and with rough gravity signature are presented. For wave estimation, the estimation cycle is chosen to be 80 sec except when v=180 km/hr, where 120 sec estimation cycle is assumed.

It is indicated in Table 7.1 that, with baseline gravity signature, both Kalman filter and wave estimation can achieve an accuracy of about 1~3 mgal (RMS), and with rough gravity signature in straight line trajectory, about 4~5 mgal (RMS) for Kalman filter and 5~7 mgal (RMS) for wave estimation is achievable. By comparing Table 7.2 with Table 7.1, one can see that the Kalman filter can largely reduce the estimation error (but not for rough field) after the linear adjustment using closure information, while the wave estimation does not reveal significant accuracy improvement, even deterioration for L-shape and circle cases.

		Straight line			L-shape	Circle
		v=360	v=180	rough	v=360	v=360
Kalman	(N)	1.157		3.653	1.413	2.775
Filter	(E)	3.157		4.310	2.068	1.462
Wave	(N)	1.738	2.388	4.650	1.154	1.980
Estimation	(E)	3.202	1.171	6.822	1.525	1.431

Table 7.1 A summary of gravity estimation errors (RMS) for different occasions without closure gravity information. (Unit: RMS--mgal; v--km/hr)

	Straight line			L-shape	Circle
	v=360	v=180	rough	v=360	v=360
Kalman (N)	1.197		4.104	1.495	0.927
Filter (E)	1.020		4.767	0.667	1.105
Wave (N)	1.375	1.866	7.297	1.832	2.700
Estimation (E)	2.598	1.532	6.655	1.436	1.879

Table 7.2 A summary of gravity estimation errors (RMS) for different occasions with closure gravity information. (Unit: RMS--mgal; v--km/hr)

All in all, through the above discussions, the following ideas have been explored and some conclusions can be drawn:

(1) The medium accuracy strapdown INS, e.g. LN-93, supplemented by the differential GPS measurements is well suited for airborne vector gravimetry. The estimable range for the gravity disturbance is mainly concentrated in the medium wavelength. With the assumed airplane speed of 360km/hr, the minimum wavelength of 45 km in baseline gravity signature and 18 km in rough gravity areas can be recovered by vector gravimetry. The maximum detectable wavelength is about 334 km in baseline gravity field and 338 km in rough areas. For smooth gravity signature, it is unlikely to recover the gravity disturbance information with a mix of the LN-93 inertial system and GPS.

(2) The gravity disturbance itself is a major error source to gravimetry, which has been clarified in the spectral domain. The bigger estimation error in the simulation for the rough gravity field verified this conclusion to some extent.

(3) With baseline gravity signature, an accuracy of about 1~3 mgal can be achieved by either Kalman filter or wave estimation for all trajectories within one hour. In straight-line survey and rough area, the wave estimation performs not as well as the Kalman filter. The Kalman filter has a good physical description of the system error states and would yield good results as long as the a prior statistical information is sufficiently known. Also the Kalman filter procedure allows sufficient time to get convergence in some systematic error estimation (e.g. gyro drifts and the azimuth error) though the actual improvement of these errors is limited in the cases discussed. The wave estimation has to deal with the state convergence problem while trying to keep the estimation cycle as short as possible for good deterministic description of the gravity disturbance. This is probably the reason that the wave estimation performs not as well as the Kalman filter when in the straight-line mission and in the rough gravity area. In the L-shape and circle trajectories, the systematic error residuals behave differently from that in straight-line mission. And the estimated error by Kalman filter turns out to be larger than that by wave estimation. The reason for this needs to be further investigated. However, one may find, there is a

consistent error trend in the Kalman filter estimation but not in the wave estimation. This explains why the estimation error with Kalman filter is reduced significantly when using closure information with linear adjustment, while the estimation error with wave estimation is not.

(4) The most appropriate estimation cycle for wave estimation varies with the vehicle speed. For a normal airplane speed (360 km/hr), the estimation cycle is about 80 sec.

It should be noted that the above analyses are based on the assumption that all survey missions are performed at the same altitude, i.e., the influence of height on the gravity information is neglected. Also the technique to determine the level of the calibration residual error at alignment needs to be further investigated. It is strongly suggested here to try to access the estimated covariance matrix during the alignment if possible. By doing so, one can make use of the correlation built up through the initial alignment to shorten the converging time of gyro drifts and figure out the level of residual error as well.

System simulations are a kind of simplification for the realistic situation. From the practical point of view, any conclusions or results from simulations could be considered as a useful guide for real tests and need to be verified in the real world.

REFERENCES

Anderson, B.D.O. and J.B. Moore, (1979): *Optimal Filtering*. Prentice-Hall, Englewood Cliffs, NJ.

Brown, R.G., (1983): *Introduction to Random Signal Analysis and Kalman Filtering*, Wiley & Sons, New York.

Brozena, J.M., G.L. Mader and M.F. Peters, (1989): Interferometeric Global Positioning System: three-dimensional Positioning Source for Airborne Gravimetry, *J. Geophys. Res.*, 12153-12162.

Brozena, J.M. and M.F. Peters, (1994): Airborne Gravity Measurement at NRL, Proc. of the International Symposium on Kinematic Systems in Geodesy, Geomatics and Navigation, Banff, Canada, Aug. 30-Sept. 2, 1994, pp. 495-506.

Colombo, O.L., (1991): The role of GPS/INS in mapping the Earth's gravity field in the 1990's. *International Association of Geodesy Symposia- Kinematic Systems in Geodesy, Surveying and Remote Sensing*, pp.463-467, Springer-Verlag, Berlin.

Colombo O.L., (1992): Airborne Gravimetry, Altimetry, and GPS Navigation Errors. In: *Proc. IAG Symp.*, From Mars to Greenland: Charting Gravity with Space and

Airborne Instruments, General Assembly of the IUGG, Vienna, 1991, Springer-Verlag, New York.

Forsberg, R. and S. Kenyon, (1994): Evaluation and Downward Continuation of Airborne Gravity Data- The Greenland Example, Proc. of the International Symposium on Kinematic Systems in Geodesy, Geomatics and Navigation, Banff, Canada, Aug. 30-Sept. 2, 1994, pp. 531-538.

Gao, Z., (1989): *Random Process in Engineering System* (in Chinese), Tsinghua University Press, Beijing.

Gelb A. (1974): *Applied Optimal Estimation,* M.I.T. Press, Massachusetts.

Gleason, D.M., (1992): Extracting Gravity Vectors from the Integration of Global Positioning System and Inertial Navigation System Data, *J. Geophys. Res.*, 97(**B6**), 8853-8864.

Gradshteyn, I.S. and I.M. Ryzhik, (1980): *Table of Integrals, Series, and Products*, Academic Press, Inc., New York, 1980.

Hammada, Y. (1995): Airborne gravimetry by GPS/INS-A comparison of filtering methods, Proc. of ION GPS-95, Palm Springs, CA, Sep 12-15, 1995.

Huddle, J.R. (1977): The Theoretical Principles for Design of the Inertial Surveyor for Position and Gravity Determinations. Proc. of the 1st Int. Symp. on Inertial Technology for Surveying and Geodesy, Ottawa, 1977, pp. 45-59.

Huddle J.R. (1988): The Rapid Geodetic Survey System (RGS), Proc. Chapman Conference on Progress in the Determination of the Earth's Gravity Field, Sept 13-16, Fort Lauderdale.

Humphrey, I. and T. Kawakami, (1996): User Friendly Bus Controller GPS/INS Integration Software Documentation, USAF Phillips Laboratory Geophysics Directorate, Mayflower Communication Co. Inc.

Jordan S.K. (1981): State-space Models of Gravity Disturbance Gradients, *IEEE Trans Aero Elec Sys*, AES-**17**(5): 610-618.

Jekeli, C., (1992): Vector Gravimetry Using GPS in Free-Fall and in an Earth-Fixed Frame, *Bulletin Geodesique*, **66**(1): 54-61.

Jekeli, C., (1993): A Review of Gravity Gradiometer Survey System Data Analyses, *Geophysics*., **58**(4), April 1993.

Jekeli, C., (1994a): Airborne vector gravimetry using precise position-aided inertial measurement units, *Bulletin Geodesique,* **69**:1-11.

Jekeli, C., (1994b): On the computation of vehicle accelerations using GPS phase accelerations. Proc. Internat. Symp. On Kinematic Systems in Geodesy, Geomatics and Navigation (KIS94), Banff, Alberta, pp.473-482.

Jekeli, C., (1995): GPS/INS Positioning and the Earth's Gravitational Field. Proceedings 1995 Mobile Mapping Symposium, Columbus, Ohio, May 24-26 1995.

Jekeli, C. and R. Garcia, (1997): GPS phase acceleration for moving-base vector gravimetry, *Journal of Geodesy*, **71**(10): 630-639.

Kay, S.M., (1988): *Modern Spectral Estimation: Theory & Application*, Prentice-Hall, Inc., Englewood Cliffs, New Jersy.

Kleusberg, A., A. Goodacre and R.J. Beach, (1989): On the use of GPS for Airborne Gravimetry. Paper Pres. at the 5th Int. Geod. Symp. on Satellite Positioning, Las Cruces, New Mexico, March 13-17, 1989.

Kleusberg, A., D. Peyton and D. Wells, (1990): Airborne Gravimetry and the Global Positioning System, Proc. IEEE PLANS 1990, Las Vegas, pp.273-278.

Knickmeyer, E.T., (1990): Vector gravimetry by a combination of inertial and GPS satellite measurements, Report No. 20035 Dept. of Surveying Engineering, Univ. of Calgary.

LaCoste, L., J. Ford, R. Bowes and K. Archer, (1982): Gravity Measurements in an Airplane Using State-of -the-Art Navigation and Altimetry. *Geophysics*, **47**(5): 832-838.

Litton System, Inc., (1985): Performance Accuracy (Truth Model/ Error Budget) Analysis for the LN-93 INU, Document No. 469414, Litton Guidance and Control Systems, January 1985.

Litton Systems, Inc., (1990): LN-93 Standard Ring Laser Gyro Inertial Navigation Unit Technical Description, Document No. 17969EX GC87-6247. Litton Guidance and Control Division, November 1990.

McLellan, James H., (1982): Multidimensional Spectral Estimation, *Proceedings of the IEEE*, **70**(9), September 1982.

Moritz, H., (1967): Kinematical Geodesy, Report No. 92, Dept. of Geodetic Science, The Ohio State University, Columbus.

Moritz, H., (1976): Covariance Functions in Least-Square Collocation, Report No. 240 Dept. of Geodetic Science, The Ohio State University, Columbus.

Nash, R.A. (1968): Effect of vertical deflections and ocean currents on a maneuvering ship. *IEEE Trans. Aerospace and Electronic Systems*, AES-**4**(5): 719-727.

Salychev, O.S., A.V. Bykovsky, V.V. Voronov, K.P. Schwarz, Z.Liu, M.Wei, J. Panenka, (1994): Determination of Gravity and Deflections of the Vertical for Geophysical Applications Using the ITC-2 Platform, Proc. of Intern. Symp. on Kinematic Sys. in Geodesy, Geomatics and Navigation, Univ. of Calgary, Banff, Canada August 30-September 2, 1994.

Salychev, Oleg S. (1995): *Inertial Surveying: ITC Ltd. Experience*, Bauman MSTU (Moscow State Technical University) Press 1995.

Salychev O.S., Schwarz K.P. and Hammada Y., (1995): An Analysis of the Wave Approach to State Vector Estimation, *IAG Symposium* G4, IUGG XXI General Assembly, Boulder, Colorado, July2-14, 1995.

Schwarz, K.P. (1984): Inertial Geodetic Survey, Lecture Notes, (translated into Chinese), Tsinghua Univ. 1984.

Schwarz, K.P. (1987): Geoid profiles from an integration of GPS satellite and inertial data, Anno XIVI. Bollettino di Geodesia e Scienze Affini - N.2, 1987, pp.117-131. Presented at the International Symposium on the Definition of the Geoid, Florence, Italy, May 26-30, 1986.

Schwarz, K.P., M.E. Cannon and R.V.C. Wong, (1989): A Comparison of GPS Kinematic Models for the Determination of Position and Velocity Along a Trajectory, *Manuscripta Geodaetica,* **14**: 345-353.

Schwarz, K.P., O. Colombo, G. Hein, and E.T. Knickmeyer (1991): Requirements for Airborne Vector Gravimetry, *Proceedings of the IAG Symposium* No. 110 'From Mars to Greenland: Charting Gravity with Space and Airborne Instruments' IUGG General Assembly, Vienna, Austria, August 11-21.

Schwarz K.P., Y. Li and M. Wei (1994): The Spectral Windows for Airborne Gravity and Geoid Determination, Proc. of Intern Symposium on Kinematic Sys in Geodesy, Geomatics and Navigation, Univ. of Calgary, Banff, Canada, August 30-September 2, 1994.

Teunissen, P.J.G. and A. Kleusberg, (1995): GPS observation equations and positioning concepts. Lecture Notes, International School GPS for Geodesy, Delft, The Netherlands, 26 March-1 April, 1995.

Wang, J. and Z. Gao, (1996): Real time estimation of position and the gravity vector with an inertial survey system, *Journal of Geodesy*, **71**: 16-20.

Wei M, M.E. Cannon & K.P. Schwarz, (1992): Maintaining Hing Accuracy GPS Positioning 'On the Fly'. IN: *Proc IEEE'92 Position, Location and Navigation Symposium*, pp. 403-411.

Wei, M. and K.P. Schwarz, (1994): An Error Analysis of Airborne Vector Gravimetry, Proc. of the International Symposium on Kinematic Systems in Geodesy, Geomatics and Navigation, Banff, Canada.